International Journal of Earth Sciences
https://doi.org/10.1007/s00531-022-02282-2

ORIGINAL PAPER

Tracing the cryptic Sardic (Ordovician) metamorphism across Alpine Europe: the Krndija region in the Slavonian Mountains, Croatia

B. Starijaš Mayer[1] · A. Zeh[2] · E. Krenn[1] · A. Gerdes[3] · F. Finger[1]

Received: 28 June 2022 / Accepted: 9 December 2022

Abstract

Results of a combined petrological, geochemical and geochronological study suggest that metasedimentary rock units in the Krndija region of the Slavonian Mountains, Croatia, were affected by at least three major tectonometamorphic imprints: during the Middle Ordovician (Sardic event), the early Carboniferous (Variscan event), and the Cretaceous (Alpine event). All three metamorphic phases are established by electron microprobe-based in-situ U–Th–Pb dating of monazite grains. The Sardic metamorphic event is additionally confirmed by a precise Lu–Hf garnet-whole-rock isochron age of 466.0 ± 2.3 Ma. Taken together, the data unveil a relatively large and well-preserved piece of the cryptic Sardic orogen in central Krndija, that we name the Kutjevo Zone. A Sardic subduction-related metamorphic event (ca. 540-580 ℃, 8–11 kbar) at ca. 466 Ma is manifested in the mineral paragenesis Ca-rich garnet plus rutile. A low degree of retrograde reequilibration suggests a subsequent fast exhumation. Low-Ca cores in some garnets and staurolite relics record a pre-HP metamorphic event that involves isobaric heating from 570 to 610 ℃ at ~ 7 kbar. We attribute this (so far undated) event to mid-crustal contact metamorphism caused by early Sardic magmatism. Southern parts of Krndija (the Gradište Zone) experienced an (additional?) clockwise *PT* evolution in Variscan times at ca. 350 Ma. Garnet formed with ilmenite during a *PT* increase from 580 ℃/5 kbar to 600 ℃/6 kbar and underwent later strong retrograde resorption. Slow Variscan exhumation resulted in andalusite formation at < 550 ℃/ < 3.8 kbar. Penetrative Alpine metamorphism was observed in low-grade phyllites in the north. The lithology and metamorphic history of the Kutjevo Zone is similar to what has been reported from the Sardic Strona-Ceneri Zone in the western Alps. Both areas expose metapelitic (metagreywacke) rocks with a pre-middle Ordovician formation age. These metasedimentary rocks are inter-layered with numerous small amphibolitic units as well as metagranitoids and were likely deposited along the active Gondwana margin, perhaps in a fore-arc position, prior to their subduction during the middle Ordovician. According to recent palaeogeographic reconstructions, both the Kutjevo Zone and the Strona-Ceneri Zone have once resided in an eastern sector of the northern Gondwana margin (i.e., in E-Armorica). We conclude that in the Middle Ordovician, important subduction activities took place in this E-Armorican segment of north Gondwana, which is today exposed in the Alps. The W-Armorican segment of north Gondwana (now exposed in the French, German, and Czech Variscides) had probably already mutated from a (Cadomian) subduction setting to an extensional (transtensional–transpressional) setting by the late Cambrian.

Keywords Slavonian Mountains · Sardic orogeny · Ordovician metamorphism · Variscan metamorphism · Alpine metamorphism · Gondwana margin

✉ F. Finger
friedrich.finger@plus.ac.at

[1] Department of Chemistry and Physics of Materials, Paris Lodron University of Salzburg, Jakob Haringerstraße 2a, 5020 Salzburg, Austria

[2] Karlsruher Institut für Technologie (KIT), Institut für Angewandte Geowissenschaften, Mineralogie & Petrologie, Adenauerring 20b76131, Karlsruhe, Germany

[3] Institute of Geoscience, University of Frankfurt, Altenhöferalle 1, 60438 Frankfurt am Main, Germany

Introduction

Significant relics of pre-Permian basement can be found in many places throughout the Alpine orogen (e.g., Schaltegger and Gebauer 1999; Thöni 1999; Eichhorn et al. 2001; von Raumer et al. 2013; Neubauer et al. 2022). These rocks constitute important mosaic pieces in the reconstruction of the Palaeozoic evolution of central Europe. In simple terms, the pre-Permian basement rocks of the Alps are often referred

Published online: 21 January 2023

to as "Variscan basement", assuming that they formed (or at least received a major tectonometamorphic imprint) during the Variscan orogeny. However, geochronological research increasingly shows that many of these rocks have a prominent Early Palaeozoic metamorphic and magmatic history (e.g., von Quadt 1992; Bussy and von Raumer 1994; Poller et al. 1997; Zurbriggen et al. 1997; Schulz et al. 2004; Franz and Romer 2007; von Raumer et al. 2013; Neubauer et al. 2022).

The Early Palaeozoic rocks represent important relics of the northern Gondwana margin, from where the central European crust is mainly derived (Linnemann et al. 2004; Nance et al. 2008; von Raumer et al. 2013). A widely accepted assumption is that the northern Gondwana margin was in a state of extension in the Early Palaeozoic (Franke et al. 2000; Franke et al. 2017) and was affected by high heat flow and rift-related magmatism (Pin and Marini 1993). However, the existence of Ordovician Barrow-type metamorphism in Alpine basement units (e.g., Biino 1995; Zurbriggen et al. 1997; Faryad et al. 2002; Franz and Romer 2007) implies that subduction processes must have played a role as well, at least locally. These Ordovician subduction activities, summarized as the Sardic tectonometamorphic phase by Handy et al. (1999), constitute a cryptic feature in the evolution of the central European crust. The debate on the significance of an orogenic phase of "Caledonian" age in Variscan Europe was first introduced by Stille (1939) to account for a Middle-Ordovician gap in the stratigraphy of SW Sardinia (Teichmüller 1931).

In this paper, we introduce another key area for the study of this "pseudo-Caledonian" orogenic phase, namely the Krndija region of the Slavonian Mountains, Croatia. Our multidisciplinary geochronological–petrological–geochemical study clearly reveals that this area contains well-preserved Sardic basement, which shares many similarities with the Strona-Ceneri Zone, the type locality for Sardic metamorphism in the Alps. Parts of Krndija were also affected by strong Variscan and by Alpine metamorphism. The systematic combination of in-situ monazite dating with thermobarometry (Schulz 2021) allows us to resolve the polymetamorphic history of this part of the Slavonian Mountains.

Geological background

The Slavonian Mountains in Croatia, subdivided geographically into the Psunj, Papuk, and Krndija regions (Fig. 1, inset), form one of the largest crystalline basement complexes within the Tertiary Pannonian Basin (Fodor et al. 1999; Pamić and Jurković 2002). In terms of the Alpine plate tectonic framework, they belong to the Tisia-Unit. This tectonic unit lies adjacent to the Southern Alps and the Dinarides (Fig. 1), and it is commonly regarded as a lithospheric fragment broken off from the European plate during the Middle Jurassic opening of the eastern branch of the Alpine Tethys (Géczy 1973; Csontos 1995; Pamić et al. 2002; Schmid et al. 2008). The Tisia-Unit came into its present-day position after complex translational and rotational movements during the Mesozoic and Cenozoic (Csontos 1995; Fodor et al. 1999; Csontos and Vörös 2004). These motions were controlled by the major tectonic contact zones of the Alpine–Carpathian–Dinaridic orogenic system, most of them representing oceanic sutures (Schmid et al. 2008). The internal structure of the Tisia-Unit encompasses three internal, southward dipping, Alpine nappe systems, called Mecsek, Villány–Bihor, and Békés–Codru, each comprising igneous and metamorphic basement rocks and post-Variscan overstep sequences (Haas and Péró 2004; Csontos and Vörös 2004; Schmid et al. 2008). The Slavonian Mountains belong to the Villány–Bihor nappe system (Fig. 1, inset).

The main crystalline lithologies of the Slavonian Mountains are mica schists, paragneisses, amphibolites, migmatites, and granites (Jamičić and Brkić 1987; Jamičić 1989). The abundant granitic rocks (Fig. 1) are generally considered to be Variscan intrusive rocks, based on field relationships and geochronological data (Pamić et al. 1988; Pamić and Lanphere 1991; Pamić and Jurković 2002). The formation ages of the metamorphic rocks (Fig. 1) have been controversially assessed in the past. Historically, an Early Palaeozoic/or late Neoproterozoic (Baikalian) age and a pre-Variscan metamorphism were envisaged for, at least, some of the rocks based mainly on stratigraphical constraints (Jamičić 1983, 1989; Jamičić and Brkić 1987). In more recent work, it was mostly suggested that the metamorphic evolution of the Slavonian Mountains is essentially Variscan (Pamić et al. 1988; Pamić and Lanphere 1991; Pamić and Jurković 2002). The significance of a very low- to low-grade metamorphic overprint during the Cretaceous has also been recently highlighted (Biševac et al. 2009, 2011; Balen et al. 2013; Starijaš Mayer et al. 2013).

Results of previous studies

Our current knowledge about the metamorphic rocks of the Slavonian Mountains relies mainly on the detailed mapping work of Jamičić (1983, 1989) and Jamičić and Brkić (1987), as well as several petrographic studies by Pamić and coauthors (e.g., Pamić et al. 1988, 2002; Pamić and Lanphere 1991). Jamičić (1983, 1988) distinguished three tectonometamorphic units in the Slavonian Mountains, termed the Radlovac, the Psunj, and the Papuk metamorphic complexes (Fig. 1).

The *Radlovac metamorphic complex* comprises a very low-grade metamorphic sequence of slates, metagreywackes, metaconglomerates, and subordinate phyllites, with some

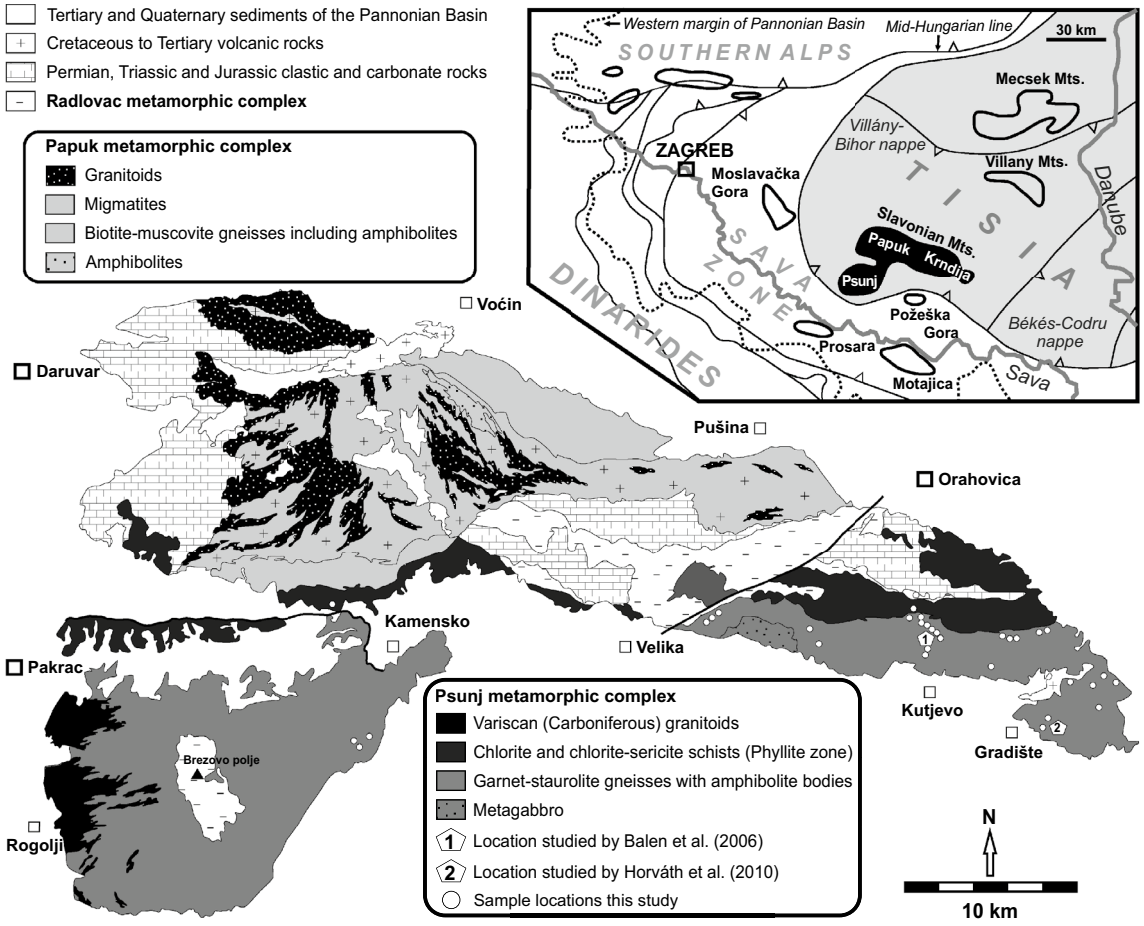

Fig. 1 Simplified geological map of the Slavonian Mountains (after Jamičić et al. 1986; Jamičić and Brkić 1987; Jamičić 1988) with inset-map showing the position of the Slavonian Mountains (black) within the Tisia Unit and the Alpine–Carpathian–Dinaric tectonic framework, respectively. Inset map slightly modified after Schmid et al. (2008)

intrusive bodies of metadiabase and metagabbro (Pamić and Jamičić 1986). Recent studies have shown that the regional metamorphic overprint is most probably of Cretaceous (Alpine) age (Biševac et al. 2009, 2011). Chloritoid schists occurring at the base of the Radlovac complex formed at conditions of 340–380 ℃/3.5–4.0 kbar (Balen et al. 2013). The rocks of the Radlovac complex overly the higher grade Psunj metamorphic complex and are themselves unconformably overlain by a clastic-carbonate succession of Late Permian and Triassic age (Jamičić 1983; Jamičić and Brkić 1987).

The *Psunj metamorphic complex* outcrops as greenschist facies metapelites (mainly phyllites, subordinate greenschists, and quartz-muscovite schists) in the north. A higher grade metapelitic unit (map name: garnet staurolite gneisses) extends toward the south (Fig. 1). The latter unit also includes garnet–chlorite–muscovite schists, garnetiferous mica schists, amphibolites, metagranitoids, metagabbros, and rare marbles. Based on thin-section observations and K–Ar mica ages, Pamić et al. (1988) and Pamić and Lanphere (1991) have interpreted the entire Psunj complex as a prograde Barrow-type metamorphic sequence of Carboniferous (Variscan) age.

The *Papuk metamorphic complex* consists of migmatites and migmatic gneisses arranged around a core of S-type granite (Pamić et al. 1988, 1996; Pamić and Lanphere 1991). The migmatitic rocks grade into an amphibolite facies metamorphic sequence mapped as biotite muscovite gneisses, which also contain garnetiferous amphibolites, paragneisses, and mica schists. According to Pamić and Lanphere (1991), the metamorphic evolution in Papuk is contemporaneous with that in Psunj, representing deeper Variscan crust affected by migmatization and granite formation.

The concept of a monocyclic Variscan metamorphic evolution of the entire Slavonian Mountains was challenged in a study of Balen et al. (2006), who investigated amphibolite, paragneiss, and mica schist samples from a locality in the Psunj metamorphic complex, ~ 3 km north of Kutjevo (Fig. 1). Only pre-Variscan monazite (420–460 Ma) was identified using electron microprobe-based monazite dating methodology. Based

on their data, Balen et al. (2006) suggested that the amphibolite facies metamorphism seen at this locality (~600 ℃, 10 kbar) has a late Ordovician or early Silurian age. Mica schists from another locality in the Psunj metamorphic complex near Gradište (Fig. 1) were studied by Horváth et al. (2010). In this study, however, only metamorphic monazite of Variscan (Early Carboniferous) age was found. Horváth et al. (2010) stated that the Variscan metamorphic evolution of this micaschist involved an early stage at ~ 630 ℃ and 7–8 kbar (recorded by garnet cores) and evolved clockwise into a penetrative crystallization stage at ~ 550 ℃ and 3–5 kbar recorded in the growth of staurolite and andalusite.

Considered together, the two local studies of Balen et al. (2006) and Horváth et al. (2010) lead to two important conclusions:

1) The Psunj metamorphic complex is obviously polymetamorphic with a Variscan and a pre-Variscan history.
2) The Variscan PT evolution appears to be different from the pre-Variscan one, in that it involves a higher thermal gradient.

Objectives of the present study

The first aim of our study is to better define the regional extent of pre-Variscan and Variscan metamorphism in the metapelite series of Krndija, using the method of *in-situ* electron microprobe (EMP) dating of monazite grains in thin section. For this purpose, about 20 samples of metapelitic rocks were collected (Fig. 1).

A second objective is to confirm the age of the pre-Variscan metamorphism by an independent dating method to obtain more precise geochronometric information than is possible with the EMP monazite dating method. To this end, we carried out Lu–Hf isochron dating of garnet fractions separated from a chlorite–muscovite–garnet schist from north of Kutjevo. Third, geochemical data are presented, which provide new constraints on the protoliths of the investigated metasedimentary rocks, as well as on the palaeotectonic environment during deposition. Based on our new geochronological data and by carefully considering the petrography of the metamorphic rocks, we can finally provide new constraints on the (poly)metamorphic history of the Slavonian Mountains. Constraints on the palaeoplate–tectonic history are also discussed.

Methods

Th–U–Pb monazite dating with the electron microprobe

Monazite analyses were carried out with a wavelength dispersive system on a JEOL-JX8600 electron microprobe at the Paris Lodron University of Salzburg, following routines described in detail in Krenn et al. (2008) and Krenn and Finger (2004). The analytical procedure considers suggestions of Pyle et al. (2002) and Jercinovic and Williams (2005) of how to optimize the precision and accuracy of the method. Single point ages and errors were calculated after Montel et al. (1996). Weighted mean ages were calculated using the Isoplot program 3.41b (Ludwig 2007) and the software IsoplotR of Vermeesch (2018).

Lu–Hf dating of garnet

Ca. 2–3 kg of chlorite–muscovite–garnet schist with euhedral garnet were processed in a jaw crusher and sieved. Three garnet fractions, weighing between 70 and 400 mg, from the 125–250 µm sieved material were handpicked under a binocular microscope, and grains with visible inclusions were excluded. These handpicked fractions were then digested in closed Teflon® vials on a 120 °C hotplate to selectively dissolve the garnet and avoid a contamination by potential zircon and rutile inclusions. The method used is described in detail by Lagos et al. (2007) and Zeh and Gerdes (2014). Note that high-pressure Parr® bombs were not used. After rinsing with Milli-Q H_2O, the garnet solutions were spiked with a mixed $^{176}Lu/^{180}Hf$ tracer for Lu and Hf concentration determinations and then digested as follows: the garnet was decomposed in $HF–HNO_3–HClO_4$ and then 10 M HCl, and the samples were dried at high temperature (fuming $HClO_4$) between each step (Lagos et al. 2007). Separation of Lu and Hf was achieved using an ion-exchange column containing Eichrom Ln-Spec resin (Münker et al. 2001). Lu and Hf isotope ratios were measured using a Finnigan Neptune MC–ICP-MS equipped with a Cetac ARIDUS™ sample introduction system at Goethe University, Frankfurt. This instrumental setup ensured high sensitivity, enabling the precise measurement of Hf isotope compositions of samples having as little as 10 ng of Hf at a signal intensity of ~ 350 mV of ^{176}Hf for a 10 ppb Hf solution. Because only 50–80% of the Yb were separated from Lu during the purification technique employed here, a correction is necessary for the interference of ^{176}Yb on ^{176}Lu (Blichert-Toft et al. 1997). The Yb interference was monitored by measuring two interference-free Yb isotopes (^{173}Yb and ^{171}Yb). Their ratio was used to apply an instrumental mass bias correction to measured $^{176}Lu/^{175}Lu$ values, assuming a $^{173}Yb/^{171}Yb$ of 1.129197 and the exponential law (Vervoort et al. 2004). This mass bias correction was also applied to the $^{176}Yb/^{171}Yb$ used for correcting the ^{176}Yb interference on ^{176}Lu. In-run statistics for the measured and corrected $^{176}Lu/^{175}Lu$ range from 0.006 to 0.01% 2 S.E. Mass bias on the Hf isotope ratios was corrected using $^{179}Hf/^{177}Hf = 0.7325$ and the exponential

law. The Hf solutions were virtually free of any Yb and Lu but contained various amounts of Ta and W. All isobaric interferences on Hf isotopes were monitored and corrected using the mass bias corrected $^{173}Yb/^{176}Yb$, $^{175}Lu/^{176}Yb$, $^{180}Ta/^{181}Ta$ and ^{183} W/^{180} W values. During the course of this study, the Lu standard yielded $^{176}Lu/^{175}Lu = 0.026550 \pm 17$ ($2\sigma \approx 0.07\%$, n = 6) and the Hf Standard JMC-475 yielded $^{176}Hf/^{177}Hf = 0.282155 \pm 12$ ($2\sigma \approx 0.6\varepsilon$, n = 6). In-run analytical uncertainty for $^{176}Hf/^{177}Hf$ was typically around $\pm 0.3\varepsilon$ or better. For the calculation of the mineral isochrons, the ISOPLOT program (Ludwig 2007) was used with a $^{176}Lu = 1.867 \times 10^{-11}$ a^{-1} (Scherer et al. 2001; Söderlund et al. 2004). For the $^{176}Hf/^{177}Hf$ uncertainties, we used quadratic additions of the reproducibility of the JMC-475 ($2\sigma = 0.6\varepsilon$) and the in-run precisions (2σ errors). Uncertainties on $^{176}Lu/^{177}Hf$ were propagated from the reproducibility of the Lu standard and the uncertainty in the spike calibration (0.15%) and multiplied by an error magnification factor that depends on the measured $^{176}Lu/^{175}Lu$. Resulting uncertainties for the $^{176}Lu/^{177}Hf$ values are about 0.20%. Repeated blank measurements yielded < 40 pg for both Lu and Hf. Epsilon Hf for whole rock was calculated using the estimated $^{176}Hf/^{177}Hf$, $^{176}Lu/^{177}Hf$ and the metamorphic age (466 Ma), as well as the CHUR parameters of Bouvier et al. (2008). The hafnium model age (two-stage model) was calculated using the measured $^{176}Lu/^{177}Lu$ and the metamorphic age (466 Ma) for the first stage. For the second stage, a $^{176}Lu/^{177}Hf$ of 0.0113 was used for the average continental crust, and a depleted mantle $^{176}Lu/^{177}Hf$ and $^{176}Hf/^{177}Hf$ of 0.0384 and 0.28325 were used, respectively (for more details, see Gerdes and Zeh 2006).

Whole-rock geochemistry

Twenty X-ray fluorescence analyses were performed on glass beads (major elements) and pressed pellets (trace elements) using a Bruker S4 pioneer crystal spectrometer device equipped with a 4 kW rhodium tube at the Paris Lodron University of Salzburg. The analyses refer to ca. 1 kg sample material. Major elements were generally determined at reduced tube energies. Counting times were chosen, such that the relative 2σ uncertainties were better than 1% for SiO_2 and Al_2O_3, and better than 5% for elements occurring at the 1–10 wt. % concentration level. For the determination of trace elements, tube conditions and counting times were optimized automatically up to 4 kW and 400 s per element to obtain a detection limit of at least 3 ppm (3σ). Typical errors (2σ) from the counting statistics are 1–2 ppm at low concentrations (< 10 ppm), ~ 5 ppm at the 100 ppm concentration level, and better than 50 ppm at the 1000 ppm level. Calibration is based on a set of 30 international rock standards (mainly USGS standards).

Thin-section studies, mineral analyses, and pressure–temperature (PT) calculations

Thin sections were first studied carefully under the optical microscope. Mineralogical and microstructural details were further investigated using a scanning electron microscope (SEM: Zeiss Ultraplus) at the Paris Lodron University of Salzburg. Mineral analyses were partly performed with an Oxford X-max 50 detector coupled to the Zeiss Ultraplus, partly with the electron microprobe Jeol JX 8600 in wavelength dispersive mode. Multiple control analyses carried out repeatedly on the same minerals of the same samples showed that both methods yield consistent results.

PT calculations were performed using various methods. For most samples, peak *PT* conditions were estimated using conventional geothermobarometers for the mineral assemblage biotite–garnet–plagioclase–muscovite (calibrations of Battacharya et al. 1992; Holland and Powell 1990). For these calculations, we used garnet rim compositions (unmodified by retrograde diffusion) and nearby grains of plagioclase (rims), biotite, and muscovite. Reported *PT* variations result from the analyses of at least five different microdomains per sample (see Table 1). In addition to conventional geothermobarometry, average *PT* conditions were estimated with the THERMOCALC software 3.33 (Powell and Holland 1998), which is based on the internally consistent thermodynamic data set file "tc-ds55.txt" and on a–X relationships described in Holland and Powell (2003) and Coggon and Holland (2002).

To obtain *PT* path information during garnet core and rim formation, *PT* pseudosections were calculated in the system $MnO–Na_2O–CaO–K_2O–FeO–MgO–Al_2O_3–SiO_2–H_2O–TiO_2$ (MnNCFMASHT) using the THERIAK-DOMINO software and the thermodynamic data set of Holland and Powell (1998) transcribed for, and implemented into, THERIAK-DOMINO by Gaidies et al. (2008). Further detailed information on calculation parameters and the used solid-solution models are given in Gaidies et al. (2008). *PT* data for different garnet core and rim domains were estimated by comparison between measured/observed and calculated mineral assemblages, modal and individual garnet compositions including mainly the grossular and pyrope components (see Figs. 4 and 5). The geochemical input data for THERIAK-DOMINO result from analyses of the ca. 2 × 3 × 1 cm rock off-cuts from the thin-section preparation (XRF analyzed) and are thus representative of the probed thin sections. H_2O was assumed to be in excess, because the samples contain chlorite and are free of carbonate. Ferric iron has not been considered, because no free

Table 1 Petrographic, thermobarometric, and geochronological data for the investigated samples

	Modal composition (vol.%)								Accessory	Estimated T (°C)		Estimated P (kbar)		Monazite age (Ma)
	Qz	Pl	Bt	Ms	Chl	Grt	St	And	minerals	Bt-Grt	Thermoc	Bt-Grt-Pl-Ms	Thermoc	
Group I														
BS 502	38	10	–	25	25	–	–	–	Ap, Rt, Tur, Zr, Mnz, Xtm		402–435		1–8*	91 ± 31 (4 grains)
BS 606	40	19	–	20	19	–	–	–	Ap, Rt, Tur, Zr, Mnz, Xtm					97 ± 26 (7 grains)
Group II														
BS 417	30	8	–	28	28	4	–	–	Ep, Rt(Ilm), Ap, Zr		552 ± 22		8.2 ± 1.2	n.m
BS 418	30	5	–	30	30	3	–	–	Ep, Rt(Ilm), Ap, Zr		542 ± 16		8.1 ± 1.0	n.m
BS 418b	29	6	–	29	31	3	–	–	Ep, Rt(Ilm), Ap, Zr		569 ± 21		8.9 ± 1.1	n.m
BS 605a	35	8	–	29	22	4	–	–	Ep, Rt(Ilm), Ap, Zr					n.m
BS 605b	30	5	–	30	30	3	–	–	Ep, Rt(Ilm), Ap, Zr					n.m
BS 416b	20	5	–	45	25	4	–	–	Ep, Rt(Ilm), Ap, Zr					n.m
Group III														
BS 416a1	54	20	12	5	5	3	–	–	Rt(Ilm), Ap, Zr, Xtm					
BS 416a2	50	20	3	13	10	3	–	–	Rt(Ilm), Ap, Zr	580–600	572 ± 22	10–11	9.2 ± 1.2	n.m
BS 607	32	27	8	12	10	10	–	–	Rt(Ilm), Ep, Ap, Zr	576–596	582 ± 24	9–11	10.1 ± 1.2	n.m
BS 412	40	20	12	20	5	2	–	–	Rt(Ilm), Ep, Ap, Zr					n.m
BS 413a	49	29	5	10	3	3	–	–	Rt(Ilm), Ap, Zr, Mnz	570–620	578 ± 22	10–12	9.9 ± 1.1	481 ± 26 (*n* = 8/12)
BS 414	30	36	5	15	8	5	–	–	Rt(Ilm), Ap, Zr	584–612	570 ± 21	10–11	9.5 ± 1.1	n.m
BS 201a	43	28	18	3	2	5	–	–	Rt(Ilm), Ep, Ap, Zr, Mnz, Xtm	570–588		10–11		474 ± 45 (n = 3/3)
BS 420	50	20	8	17	ac	4	ac	–	Rt(Ilm), Ilm, Ap, Zr, Mnz	589–603	605 ± 45	8–10	10.0 ± 1.9	470 ± 36 (*n* = 9/12)
BS 419b	15	5	10	50	10	8	2	–	Rt(Ilm), Ilm, Ap, Sil, Zr, Mnz	592–618	595 ± 26	8–10	8.7 ± 1.2	471 ± 22 (*n* = 10/15)
BS 203a	51	18	18	4	2	6	–	–	Rt(Ilm), Ep, Ap, Zr, Mnz	574–606	617 ± 47	9–11	10.8 ± 1.7	466 ± 26 (*n* = 7/11)
BS 203b	43	20	19	5	2	10	–	–	Rt(Ilm), Ap, Ep, Zr, Mnz	577–601		10–11		465 ± 34 (n = 4/6)
Group III mylonite samples														
BS 423	36	18	11	16	8	10	–	–	Rt(Ilm), Ilm, Ap, Zr, Mnz, Xtm	400–450•	430-465 [m]		1–8 [m] *	372 ± 26 (*n* = 6/11)
BS 505	29	20	25	15	5	5	–	–	Rt(Ilm), Ilm, Ttn, Ep, Ap, Tur, Zr, Mnz		404 ± 30 [m]		5.6 ± 1.1 [m]	
Group IV														
BS 407	25	35	6	17	14	2	–	–	Ilm, Ttn, Ep, Ap, Tur, Zr					n.m
BS 408a	30	30	11	15	12	1	–	–	Ilm, Ttn, Ep, Ap, Tur, Zr, Mnz, Xtm					354 ± 16 (*n* = 9/14)
BS 609	30	27	15	10	10	7	–	–	Ilm, Ttn, Ep, Ap, Tur, Zr	575–581	586 ± 33		6.5 ± 1.6	n.m
BS 410	36	20	10	20	10	3	–	ac	Ilm, Ttn, Ep, Ap, Zr	493–520	556 ± 22	4–5	4.9 ± 1.1	n.m
BS 202c	38	10	20	15	10	4	1	2	Ilm, Ttn, Ep, Ap, Tur, Zr, Mnz					356 ± 23 Ma[a]
BS 411a	35	10	17	22	11	4	ac	ac	Ilm, Ttn, Ep, Ap, Zr, Mnz					
BS 411c	45	10	20	10	10	4	–	ac	Ilm, Ttn, Ep, Ap, Tur, Zr, Mnz	512–534	565 ± 26	5–6	5.6 ± 1.0	351 ± 14 (*n* = 10/16)

m refers to the mylonitic parageneses Qtz–Ms–Chl–Ab–Ilm–Ttn. • Y-in-monazite thermometry. Given ages are weighted means of several monazite analyses per sample (n = number of analyzed grains/points)

n.m. no monazite, *a* age according to Horváth et al. (2010), *Rt(Ilm)* rutile partly replaced by ilmenite

*Data refer to single thermometers (1–8 kbar; no intersection)

ferric iron phases like hematite or magnetite were found, and the hematite component in ilmenite is negligible.

In addition, the Y-in-monazite thermometer of Heinrich et al. (1997) was used.

Petrographic data

The metapelitic rocks from the Krndija area can be divided into four petrographic groups. Each group is defined by a distinct mineral assemblage and crops out in a distinct regional zone (Fig. 2).

Group I metapelites comprise fine-grained phyllites from the northern part of the Psunj metamorphic complex. The regional distribution of these phyllites is well defined in the existing geological map (phyllite zone in Fig. 1). Parts of the phyllite zone are presently unaccessible due to landmines from the Yugoslavian war. We collected two samples (BS 502 and BS 606) of finely folded greenish-gray phyllites (Fig. 2). Both consist of ~ 40% quartz, ~ 20% chlorite, ~ 20% muscovite, and 10–20% albite. Accessory minerals are apatite, rutile, tourmaline, zircon, xenotime, and monazite. PT estimates carried out with THERMOCALC and the yttrium-in-monazite thermometer (Heinrich et al. 1997) indicate lower-to-middle greenschist facies metamorphic conditions of about 400–450 °C (Table 1), consistent with the phyllitic rock texture (Fig. 3a) and the general absence of biotite and garnet.

Group II metapelites: This rock type outcrops along the road from Kutjevo to Orahovica (Figs. 1, 2). The fine-grained, greenish-gray rocks contain small garnet porphyroblasts (3–4 vol. %) embedded in a chlorite–muscovite–quartz matrix (Fig. 3b). A few albite crystals and accessory epidote grains are present in the matrix as well, but there is no biotite. Further accessory minerals are rutile, ilmenite, apatite, and zircon. Rutile grains are commonly mantled by ilmenite.

From our sampling (Fig. 2), it would appear that group II metapelites form a ~ 300 m-thick sheet in the footwall of the phyllite zone. However, these rocks are not delineated as a discrete lithological unit in official maps and it is, therefore, unclear whether they extend along the entire southern margin of the phyllite zone or constitute only a local lens. Pamić and Lanphere (1991) briefly referred to this rock type as a lower-T equivalent of the Grt–Bt–Ms schists, which are exposed further to the south (our group III metapelites), and transitional in metamorphic grade to the phyllites to the north.

The garnet in group II metapelites is almandine-rich (Alm = 55–63 mol%). It shows a weak zoning with an inner domain that is slightly lower in calcium (Grs = 13 mol%) than the rim domain (Grs = 17 mol.%; Fig. 4a; Table 2). The spessartine component decreases relatively steadily from core to rim (25–13 mol%), whereas the almandine and pyrope components increase, as does the Fe/Mg. The observed zonation patterns indicate prograde garnet growth. Results of geothermobarometry and *PT* pseudosection modeling define a nearly isothermal pressure increase during garnet growth from 530 ℃/7.5 bar to 540–570 ℃ at 9.0 kbar (cf. Figure 4a, 5a, Table 1).

Group III metapelites are fine- to medium-grained mica schists to gneisses, which typically contain the assemblage Grt–Bt–Ms–Chl–Pl–Qtz–Rt, with quartz and plagioclase being volumetrically dominant (Table 1). In rare places, minor amounts of staurolite are also present. Group III mica schists occur along a ca. 25 km-long and 2 km-wide zone north of Kutjevo (Fig. 2). They grade into the biotite-free group II metapelites toward the north. The sampling site of Balen et al. (2006) refers to a locality in the middle part of this group III metapelite zone.

The abundance of biotite (3–19 vol.%) and the ubiquitous (2–10 vol.%), strongly zoned garnet prophyroblasts with

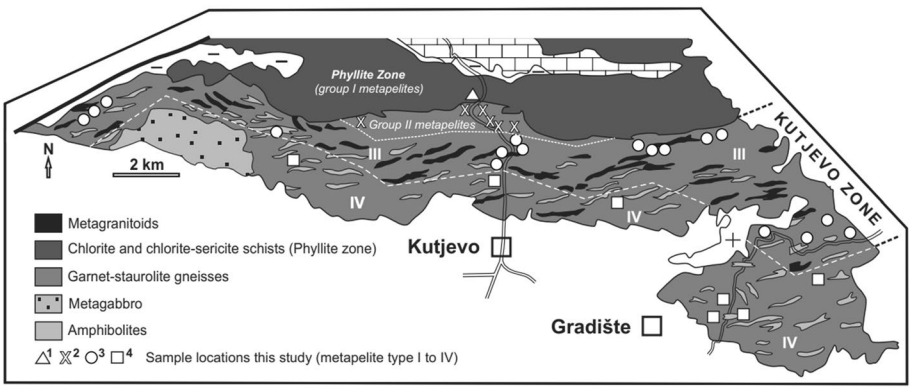

Fig. 2 Geological map of the Krndija region (eastern part of the Psunj metamorphic complex) showing the regional distribution of group I, II, III, and IV metapelites as defined in this study. Rock legend after Jamičić and Brkić (1987). Note that group II, III, and IV metapelites were previously mapped as one unit. The general dip of the rocks is toward the north. The phyllite zone occupies the hanging wall position of the complex

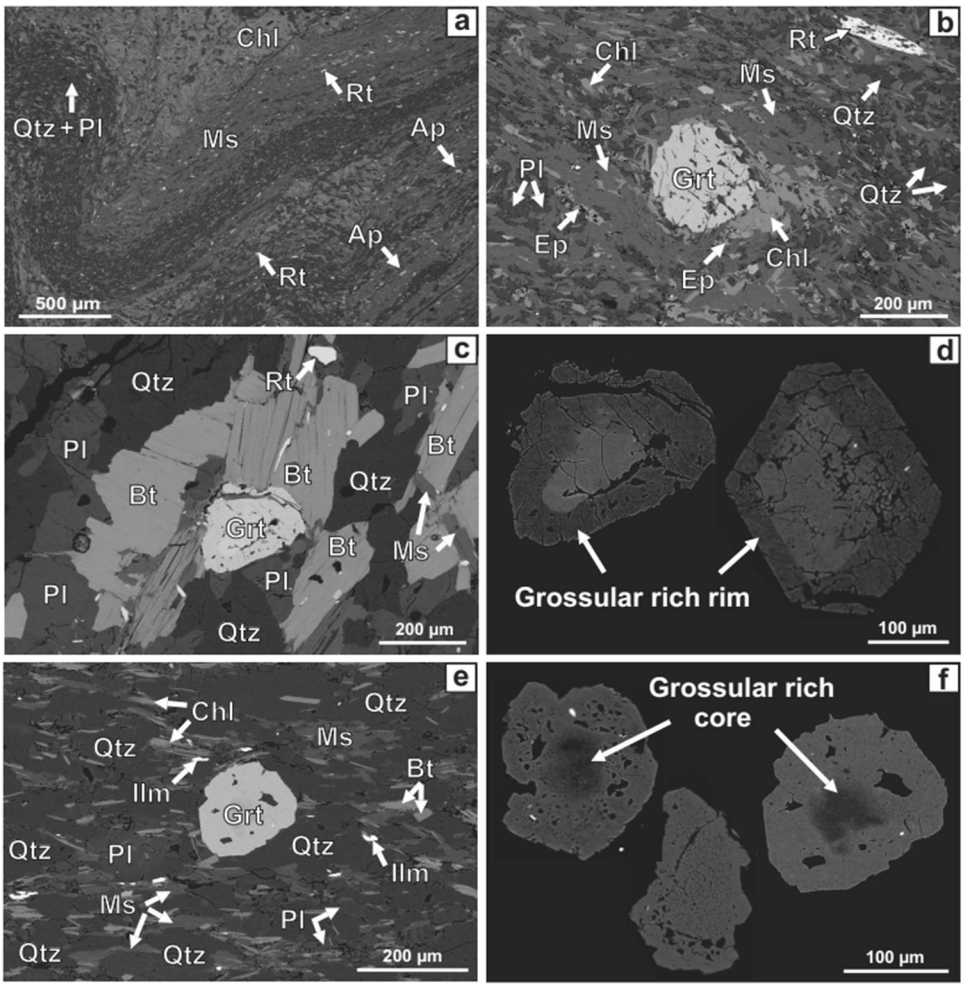

Fig. 3 Backscattered electron (BSE) images illustrating microstructures and typical garnet zonation patterns in the studied metapelite samples: **a**, **b** fabrics of group I and II metapelites (samples BS 502 and BS 418); **c**, **d** rock fabric and garnet zonation in group III metapelites (sample BS 203a); **e**, **f** rock fabric and garnet zonation in group IV metapelites (sample BS 411c)

euhedral grossular-poor cores (Grs = 7–9 mol.%) surrounded by grossular-rich rims (Grs = 20–25 mol.%) distinguish group III metapelites from group II metapelites. Muscovite contents vary mostly between 3 and 20 vol.% and chlorite contents between 1 and 10 vol.%. Euhedral rutile crystals are a characteristic accessory mineral in group III metapelites and are up to 500 µm in size. Four ca. 100 µm-sized staurolite grains are identified in two samples (BS 419b, 420). They have ilmenite inclusions(!) and are marginally resorbed and surrounded by newly formed muscovite and chlorite. In addition, a tiny 20 µm staurolite inclusion was identified in a Grs-poor garnet core.

The garnet crystals of group III metapelites are commonly euhedral (Fig. 3) with no substantial replacement by mica or chlorite obvious. Microtextures suggest that the garnet rims grew in equilibrium with most of the matrix minerals (except staurolite). The typically euhedral, angular, and unresorbed, Grs-poor garnet cores are of variable size and, in places, occupy more than two-thirds of the garnet porphyroblast (Fig. 3). Some of these cores contain small ilmenite inclusions. No rutile inclusions were observed.

In many cases, the cores are internally weakly zoned with grossular and spessartine contents decreasing from the center outwards (Fig. 4b), while the pyrope component increases. A severe chemical discontinuity is everywhere observed at the core-rim contact; grossular contents suddenly increase four- or fivefold, whereas both pyrope and almandine components significantly decrease. Interestingly, there is no great change in the spessartine content between core and rim, implying that the older garnet generation was not subjected to significant resorption before the grossular-rich rim started to grow.

The observed garnet zonation patterns, together with the results of geothermobarometry and PT pseudosection calculations, point to a fairly complex PT history of the host rock. Good agreement between measured and modeled garnet compositions is obtained for the low-Ca garnet cores by assuming a nearly isobaric temperature increase from 575 to 600 °C at 7 kbar (event M1). The zonation pattern of the Ca-rich garnet rim (event M2) is consistent with a clockwise PT evolution from 570 °C/10 kbar over 575 °C/11 kbar to 585 °C/10 kbar (thermal peak). The peak *PT* conditions at the end of the clockwise PT loop overlap, within error, with

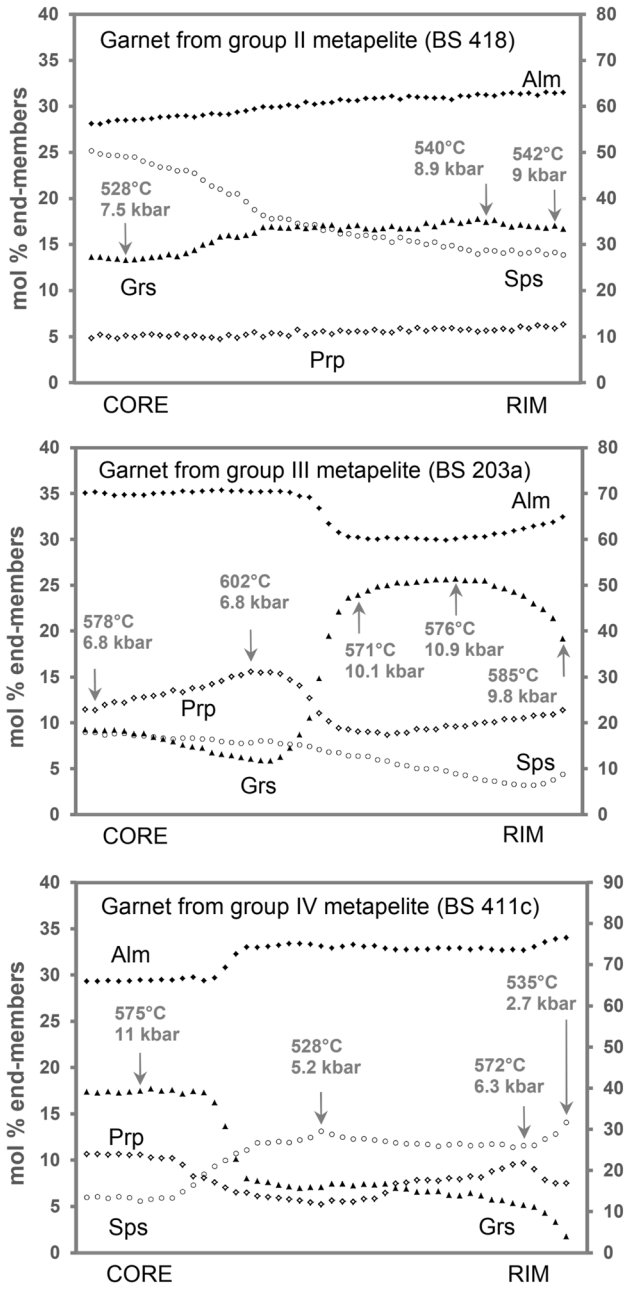

Fig. 4 Typical garnet zonation patterns in group II, III, and IV metapelites. Almandine scale on right side. P–T estimates for various steps of garnet formation rely on Grs and Prp contents in comparison to calculated isopleths in pseudosections (Fig. 5)

those obtained by the conventional geothermobarometry for unretrogressed group III metapelites (570–620 ℃/9–11 kbar, see Table 1). These PT data are in good agreement with those published by Balen et al. (2006). It could be argued that the samples from the north of the "Kutjevo" zone (Fig. 2), collected close to the group II metapelites (BS 412-416), record slightly lower temperatures than samples

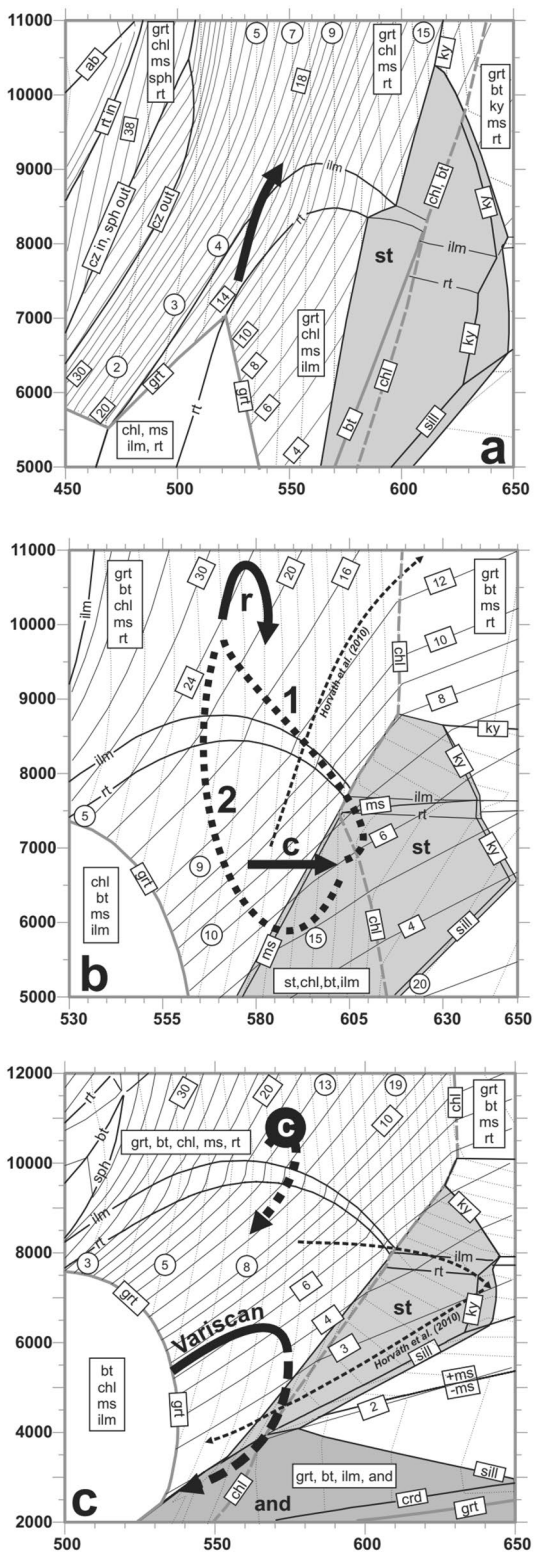

Fig. 5 Pseudosections for group II, group III and group IV metapelites (samples BS 418, BS 203a, BS 411c). Black arrows refer to P–T data derived from garnet zonation and observed mineral reactions (c: garnet cores, cf. Figure 4). Two possible P–T evolutions 1 and 2 are shown in **b** and discussed in the text. **c** P–T evolution of group IV metapelites during the Variscan. The garnet cores in these rocks may be of Ordovician age and likely traveled an independent P–T loop. Thin dashed arrows: P–T paths suggested by Horváth et al. (2010) for group III and IV metapelites

Table 2 Representative mineral compositions in studied samples

a: Representative garnet analyses from the metapelites. Selected analyses correspond to Fig. 4

	Group II (BS 418)			Group III (BS 203a)					Group IV (BS 411c)			
	Core	Rim	Rim	Core	Core	Rim	Rim	Rim	Core	Rim	Rim	Rim
SiO_2	37.01	37.17	37.00	37.31	37.21	37.59	37.74	37.44	37.44	36.61	37.00	36.66
Al_2O_3	20.94	21.03	20.91	21.13	21.06	21.28	21.36	21.19	21.15	20.69	20.89	20.72
MgO	1.28	1.41	1.47	2.86	3.92	2.30	2.44	2.89	2.68	1.29	2.41	1.85
FeO	25.31	27.76	27.96	31.40	31.53	27.22	27.23	29.25	29.85	32.67	32.63	33.58
MnO	10.76	6.31	6.22	3.95	3.50	2.85	2.00	1.97	2.49	5.68	5.07	6.10
CaO	4.62	6.05	5.91	3.20	2.02	8.41	9.08	6.75	6.15	2.43	1.79	0.60
Total	99.91	99.72	99.48	99.86	99.24	99.64	99.85	99.48	99.76	99.38	99.80	99.51
[O]	24	24	24	24	24	24	24	24	24	24	24	24
Si	5.995	6.001	5.994	5.999	5.995	5.998	5.996	5.992	5.994	5.999	5.999	6.001
Al	3.997	4.001	3.993	4.003	3.998	4.002	3.999	3.995	3.991	3.996	3.992	3.998
Mg	0.308	0.339	0.356	0.686	0.941	0.546	0.578	0.688	0.640	0.316	0.582	0.452
Fe	3.428	3.748	3.787	4.221	4.246	3.632	3.617	3.913	3.995	4.477	4.424	4.597
Mn	1.476	0.863	0.854	0.538	0.477	0.385	0.269	0.267	0.337	0.789	0.696	0.846
Ca	0.801	1.047	1.026	0.552	0.349	1.438	1.546	1.156	1.054	0.426	0.311	0.105
Grs	13	17	17	9	6	24	26	19	17	7	5	2
Prp	5	6	6	11	16	9	10	11	11	5	10	8

b: Representative analyses of plagioclase from the metapelites

	Group I		Group II				Group III		Group IV			
	BS 606		BS 417		BS 418		BS 203a	BS 607	BS 410			BS 411c
	Pl 1	Pl 2	Pl 1	Pl 2	Pl 1	Pl 2	Pl 1	Pl 1	Pl 1	Pl 2 c	Pl 2 r	Pl 1
SiO_2	68.35	66.13	67.77	65.77	68.01	65.62	62.41	63.95	64.67	67.80	64.68	64.36
Al_2O_3	19.39	18.95	19.66	21.14	19.72	21.46	23.49	22.41	22.05	19.63	21.85	22.19
CaO	0.00	0.44	0.54	2.19	0.39	2.33	4.86	3.52	2.97	0.43	2.95	3.26
Na_2O	11.71	11.37	11.49	10.42	11.50	10.37	8.96	9.67	9.97	11.53	10.02	9.86
Total	99.45	96.90	99.45	99.53	99.62	99.77	99.72	99.56	99.67	99.39	99.50	99.67
[O]	8	8	8	8	8	8	8	8	8	8	8	8
Si	2.999	2.985	2.979	2.901	2.982	2.889	2.770	2.832	2.856	2.981	2.861	2.845
Al	1.002	1.008	1.018	1.099	1.019	1.113	1.229	1.169	1.148	1.017	1.139	1.156
Ca	0.000	0.021	0.025	0.104	0.018	0.110	0.231	0.167	0.140	0.020	0.140	0.155
Na	0.997	0.995	0.979	0.891	0.978	0.885	0.771	0.830	0.854	0.983	0.859	0.845
Ab	100	98	97	90	98	89	77	83	86	98	86	85
An	0	2	3	10	2	11	23	17	14	2	14	15

c: Representative biotite analyses from the metapelites

	Group III			Group IV		
	BS 203a	BS 420	BS 607	BS 410	BS 411c	BS 609
	Bt 1	Bt 1	Bt 1	Bt 1	Bt 1	Bt 1
SiO_2	37.65	37.46	38.19	36.38	36.65	37.63
TiO_2	1.58	1.48	1.39	1.59	1.62	1.61
Al_2O_3	18.84	18.30	18.41	20.06	18.78	17.83
MgO	12.01	10.15	12.20	9.69	9.19	11.31
FeO	17.04	20.14	17.20	19.74	21.49	19.00
K_2O	8.98	8.88	9.07	8.87	8.97	9.24
Total	96.10	96.42	96.46	96.33	96.70	96.62
[O]	22	22	22	22	22	22

Table 2 (continued)

c: Representative biotite analyses from the metapelites

	Group III			Group IV		
	BS 203a	BS 420	BS 607	BS 410	BS 411c	BS 609
	Bt 1	Bt 1	Bt 1	Bt 1	Bt 1	Bt 1
Si	5.565	5.600	5.625	5.436	5.510	5.600
Ti	0.175	0.167	0.154	0.179	0.184	0.181
Al	3.281	3.225	3.195	3.534	3.327	3.127
Mg	2.645	2.262	2.678	2.159	2.059	2.507
Fe	2.106	2.518	2.119	2.466	2.702	2.364
K	1.693	1.694	1.704	1.690	1.721	1.755

d: Representative muscovite analyses from the metapelites

	Group I		Group II		Group III		Group IV	
	BS 502	BS 606	BS 417	BS 418	BS 203a	BS 607	BS 410	BS 411c
	Ms 1	Ms 2	Ms 1	Ms 2	Ms 1	Ms 2	Ms 1	Ms 2
SiO_2	45.73	45.60	45.90	45.33	45.52	45.88	45.93	45.76
TiO_2	0.48	0.46	0.24	0.31	0.55	0.69	0.45	0.47
Al_2O_3	35.55	33.59	34.59	34.95	34.99	34.81	36.09	35.87
MgO	1.45	1.39	1.25	1.07	1.38	1.45	0.83	1.01
FeO	1.57	3.03	2.87	2.65	1.42	1.32	1.70	1.41
Na_2O	0.60	0.52	0.95	1.00	1.12	0.98	1.32	1.20
K_2O	10.45	10.69	9.88	10.07	10.27	10.34	9.47	9.88
Total	95.83	95.28	95.68	95.39	95.26	95.46	95.79	95.58
[O]	22	22	22	22	22	22	22	22
Si	6.070	6.147	6.128	6.077	6.084	6.112	6.075	6.073
Ti	0.048	0.046	0.024	0.032	0.056	0.070	0.044	0.047
Al	5.562	5.337	5.442	5.521	5.511	5.465	5.626	5.610
Mg	0.286	0.279	0.249	0.213	0.275	0.287	0.164	0.199
Fe	0.174	0.342	0.320	0.297	0.159	0.147	0.188	0.156
Na	0.154	0.136	0.247	0.261	0.290	0.253	0.340	0.308
K	1.769	1.838	1.683	1.721	1.750	1.757	1.598	1.672

e: Representative chlorite analyses from the metapelites

	Group I				Group II			Group III			Group IV	
	BS 502		BS 606		BS 417		BS 418	BS 423	BS 505	BS 607	BS 410	BS 411c
	Chl 1	Chl 2	Chl 1	Chl 2	Chl 1	Chl 2	Chl 1	Chl 1	Chl 1	Chl 1	Chl 1	Chl 1
SiO_2	25.33	25.41	25.14	24.84	24.78	24.15	24.40	25.62	26.65	26.07	24.26	25.06
Al_2O_3	22.22	22.41	22.31	22.18	23.65	23.35	22.89	23.11	21.23	21.89	23.61	23.09
MgO	15.13	15.05	13.01	13.34	13.85	13.27	13.14	16.30	16.93	16.52	13.08	13.24
FeO	24.80	24.18	26.90	26.99	25.63	26.11	27.11	22.81	22.41	22.74	26.45	26.73
MnO	0.38	0.00	0.00	0.38	0.00	0.45	0.47	0.00	0.37	0.00	0.00	0.00
Total	87.86	87.05	87.36	87.72	87.91	87.33	88.01	87.85	87.61	87.21	87.40	88.11
[O]	28	28	28	28	28	28	28	28	28	28	28	28
Si	5.312	5.346	5.343	5.283	5.199	5.140	5.178	5.295	5.522	5.431	6.075	6.073
Al	5.489	5.556	5.589	5.559	5.849	5.856	5.727	5.630	5.185	5.374	5.626	5.610
Mg	4.728	4.721	4.123	4.228	4.330	4.208	4.157	5.022	5.229	5.129	0.164	0.199
Fe	4.349	4.253	4.806	4.800	4.497	4.646	4.811	3.943	3.883	3.949	0.188	0.156
Mn	0.067	0.000	0.000	0.068	0.000	0.082	0.085	0.000	0.066	0.000	0.340	0.308

Table 2 (continued)

f: Representative staurolite analyses from the metapelites

	Group III			
	BS 419b		BS 420	
	St 1	St 2	St 1	St 2
SiO_2	27.15	27.20	27.13	27.16
TiO_2	0.00	0.53	1.20	0.76
Al_2O_3	51.92	51.84	51.17	51.55
MgO	2.05	2.11	1.59	1.60
FeO	15.18	14.80	13.96	14.27
ZnO	1.78	1.88	3.09	2.90
Total	98.08	98.37	98.14	98.25
[O]	48	48	48	48
Si	7.988	7.974	7.997	7.995
Ti	0.000	0.117	0.265	0.168
Al	18.003	17.907	17.775	17.885
Mg	0.899	0.922	0.697	0.702
Fe	3.734	3.629	3.442	3.513
Zn	0.387	0.408	0.673	0.630

from the south; however, the difference is not considered enough to be conclusive.

The derived PT path sections for group III metapelites imply that staurolite + ilmenite (observed in 2 samples) were stable phases during formation of the low-Ca garnet cores but became unstable during formation of the Ca-rich garnet rims (see Fig. 5b). This interpretation is consistent with the above-mentioned observation that staurolite has only an isolated occurrence in the rocks, is everywhere partially replaced by muscovite and chlorite, and, in one case, is preserved as an inclusion in a garnet core.

It is important to note that there is not much retrograde alteration of most of the group III samples. Garnet porphyroblasts are typically perfectly euhedral and biotite is only rarely chloritized. This indicates that rock exhumation was under (most likely dry) conditions that did not favor retrograde mineral reactions and fast enough to prevent significant volume diffusion (see also the discussion in Horváth et al. 2010). The only evidence for a retrograde reaction in group III metapelites is the partial replacement of rutile by ilmenite, which must have happened during decompression.

Significant retrogression of group III metapelites is only observed along discrete shear zones/bands, which cut the main foliation at an oblique angle (samples BS 423 and 505 in Table 1). These shear bands are commonly filled with synkinematic chlorite, muscovite, quartz, and albite, and biotite is absent. Garnet porphyroblasts are commonly replaced by chlorite. Retrograde deformation also produced chains of small, aligned garnet clasts within the shear bands. Thermobarometric calculations for the shear zone minerals yield middle greenschist facies PT conditions of 400–460 ℃ and 5.5 kbar (Table 1).

Group IV metapelites: Mica schist samples collected in the southern part of the Krndija area are macroscopically not much different from group III metapelites (note the similar modal contents in Table 1). Nevertheless, these rocks carry a completely different type of garnet with low grossular content. Importantly, rutile is widely absent and ilmenite is abundant in these rocks, which sets them apart from group III metapelites. A further petrographic difference to group III metapelites is the widespread presence of small amounts (< 1 vol.% in most samples) of late-stage andalusite porphyroblasts intergrown with large chlorite crystals. In general, group IV metapelites have a finer grain size than group III metapelites (Fig. 3), and the peak mineral assemblage exhibits a comparably much stronger degree of retrogression. Garnet is commonly surrounded by a biotite–chlorite reaction seam. Staurolite, where present, occurs exclusively as small grains in the matrix and nowhere is it included in garnet. Hence, it is interpreted to be younger than the garnet.

Most garnet porphyroblasts are grossular-poor (Grs < 7 mol.%), but a few contain rounded-to-unregular-shaped (probably strongly resorbed), inherited cores with a higher grossular (15 mol.%) and pyrope (Py = 11 mol.%) content relative to the adjoining rim zones (Fig. 4). The cores themselves lack any obvious internal zonation.

The more common, core-free garnet is typically weakly zoned with a slight increase of the pyrope component, and

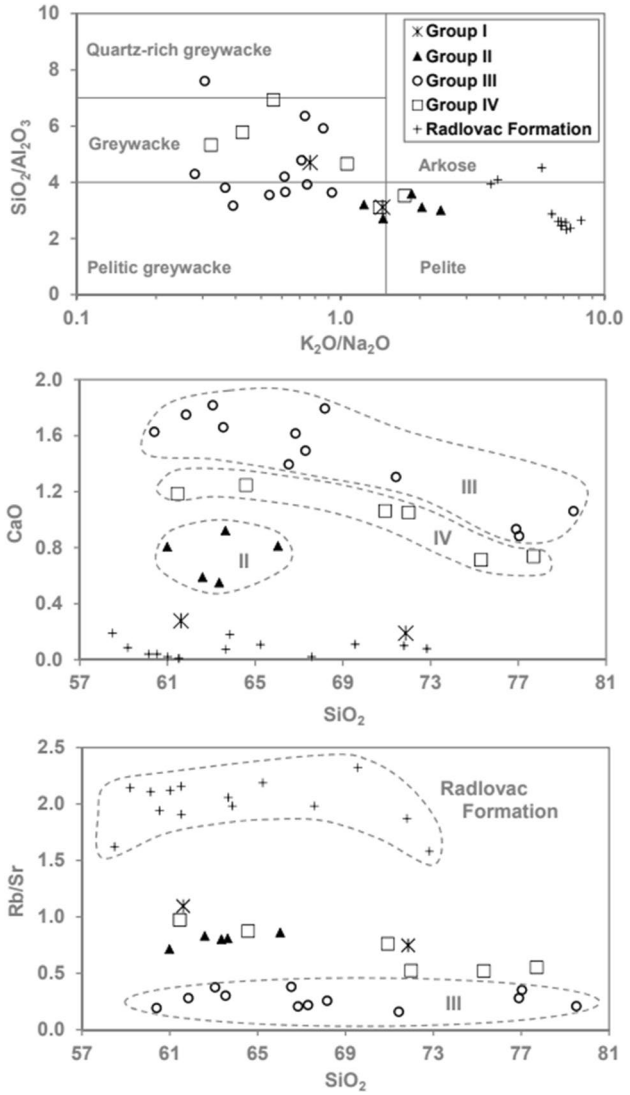

Fig. 6 Geochemical composition of metapelites from the Krndija region shown in a SiO_2/Al_2O_3 vs K_2O/Na_2O diagram after Wimmenauer (1984), and in CaO vs SiO_2 and Rb/Sr vs SiO_2 diagrams. Major elements are normalized to 100% before being plotted. Metapelites of group I to IV have different protolith compositions, implying that they belong to different stratigraphic series. The Radlovac Formation, which is shown for comparison, comprises sedimentary rocks with significantly higher Rb/Sr ratios

decrease in the spessartine and grossular components from the center to the rim of the grains. A slight increase of the spessartine component at the edges of these garnet grains is considered a chemical modification due to back-diffusion. The rims around the high Ca cores show comparable chemical zonation patterns as in the core-free garnet grains (Fig. 4).

Results of geothermobarometry and PT pseudosection modeling suggest that the rare Ca-rich cores formed at PT conditions of 580 °C/11 kbar, and the dominant low-Ca garnet porphyroblasts (or overgrowths) formed during a clockwise PT evolution from 530 °C/ 5 kbar to 570 °C/6 kbar (Fig. 5). The widespread growth of tiny staurolite and andalusite grains in the matrix is evidence that the metamorphic crystallization continued along a retrograde path from the staurolite into the andalusite field, whereby both garnet and staurolite became resorbed and replaced by chlorite and mica. This alteration very likely caused the observed back-diffusion of Mn into the outermost garnet rims. Due to continuous recrystallization of the rocks during decompression, results of conventional thermobarometry must be viewed with caution. Nevertheless, the obtained PT data (Table 1) are consistent with those obtained from the garnet zonation patterns (Fig. 5).

Geochemical composition of the metasedimentary rocks of the Krndija region

The SiO_2/Al_2O_3 vs K_2O/Na_2O discrimination diagram of Wimmenauer (1984) suggests mainly pelitic protoliths for group II metapelites and greywacke protoliths for groups I, III and IV metapelites (Fig. 6). However, notable chemical differences are discernible between group III and group IV metapelites in terms of CaO contents and Rb/Sr ratios (Fig. 6, Table 3). CaO and Sr contents are significantly higher in group III metapelites and are taken to reflect a higher proportion of detrital plagioclase in the sedimentary protoliths.

For comparison, we have also plotted data from metasedimentary rocks in the Radlovac formation (Biševac et al. 2009, 2013; Balen et al. 2013). These are generally clay-rich, feldspar-poor pelites (Fig. 6). Group I metapelites, unfortunately represented by only two samples, are Ca poor similar to the Radlovac metasedimentary rocks but lack the very high Rb/Sr ratios that characterize the latter.

The diagram of Bhatia and Crook (1986) indicates that most of the precursors to the Krndija metapelites were deposited in an active plate margin environment or, more specifically, in a continental island arc environment (Fig. 7).

Th–U–Pb electron microprobe dating of monazite

Group I metapelites: The two samples taken from the phyllite zone contain several, although generally small, monazite grains. Measured Th-U–Pb dates (Table 5) are combined to yield weighted mean ages of 91 ± 31 Ma (BS 502) and 97 ± 26 Ma (BS 606), constraining monazite crystallization to the Cretaceous. Yttrium contents in the monazite grains are generally low (< 0.5 wt.% Y_2O_3). Application of Y-in-monazite thermometry (Heinrich et al 1997) indicates that the monazite formed at temperatures of around 400–450 °C,

Table 3 Geochemical data for metapelites from the Krndija region

Sample	Group I		Group II		Group III		Group IV		Radlovac Formation	
	BS502	BS 606	BS 418	BS 605a	BS 420	BS 203a	BS 202c	BS 411c	BS 601	BS 603
SiO_2	59.76	70.13	59.18	63.97	75.40	66.70	68.72	75.90	67.17	61.49
Al_2O_3	19.23	14.94	21.83	17.83	11.86	13.96	14.74	10.95	17.09	23.57
MnO	0.07	0.05	0.09	0.08	0.04	0.13	0.07	0.08	0.02	0.06
MgO	4.18	1.75	2.13	2.17	1.22	3.02	2.01	1.54	2.24	0.55
CaO	0.27	0.19	0.78	0.79	0.86	1.75	1.03	0.72	0.11	0.32
Na_2O	2.01	2.67	2.64	1.75	2.46	3.08	2.21	2.55	1.15	0.54
K_2O	2.89	2.04	3.82	3.24	1.80	2.19	2.34	1.41	4.26	3.62
TiO_2	0.83	0.73	0.84	0.76	0.50	0.78	0.68	0.58	0.59	1.07
P_2O_5	0.17	0.15	0.10	0.16	0.07	0.17	0.13	0.11	0.10	0.41
Fe_2O_3	7.59	4.95	5.62	6.13	3.68	6.08	4.97	3.85	3.83	4.68
LOI	3.40	2.48	3.34	2.96	1.88	2.04	2.43	1.68	3.32	3.26
Total	100.39	100.07	100.37	99.83	99.76	99.88	99.32	99.36	99.88	99.58
Ba	578	361	683	667	266	581	441	309	701	1951
Ce	67	83	26	54	33	44	47	43	46	71
Cl	62	39	b.d.l	57	38	69	56	b.d.l	39	113
Co	17	15	14	17	7	16	12	11	10	b.d.l
Cr	111	76	93	78	45	99	82	79	53	151
Ga	23	15	25	19	12	14	17	13	17	30
Gd	b.d.l	4	4	4	6	7	6	5	4	10
La	34	31	21	23	31	31	27	25	15	51
Nb	13	12	15	12	8	9	11	10	9	20
Nd	17	23	9	20	28	36	29	19	19	53
Ni	36	26	43	41	23	41	33	25	29	33
Pb	8	5	21	13	11	15	9	9	9	7
Rb	108	75	127	120	53	72	72	30	135	217
Sc	20	13	18	15	7	17	22	11	12	19
Sn	10	8	b.d.l	4	7	5	7	b.d.l	8	7
Sr	99	100	178	139	150	279	95	55	58	110
Th	10	13	8	11	4	11	6	7	9	19
V	138	83	144	112	61	101	104	77	79	174
W	7	8	4	10	5	5	7	8	6	12
Y	25	23	18	18	15	24	24	20	15	55
Zn	95	75	84	96	54	76	74	53	53	45
Zr	193	347	182	206	171	182	208	222	174	220
Rb/Sr	1.09	0.75	0.71	0.86	0.35	0.26	0.76	0.55	2.32	1.98
SiO_2/Al_2O_3	3.11	4.69	2.71	3.59	6.36	4.78	4.66	6.93	3.93	2.61
K_2O/Na_2O	1.44	0.77	1.45	1.86	0.73	0.71	1.06	0.56	3.71	6.68

XRF analyses; major elements in wt%; trace elements in ppm

LOI Loss on ignition, *b.d.l.* below detection limit

consistent with the other thermobarometric estimates for the rocks (Table 1). The Cretaceous monazite ages are interpreted to date the timing of low-grade metamorphism of the phyllite zone.

Group II metapelites: Although five samples have been carefully screened, monazite was not detected in group II metapelites.

Group III metapelites: Accessory monazite is common in these samples and grains from seven samples were analyzed. The grains are typically 5–20 μm in size, round-to-subhedral, and are evenly disseminated throughout the rock matrix. Some of the monazite grains are enclosed in garnet rim zones.

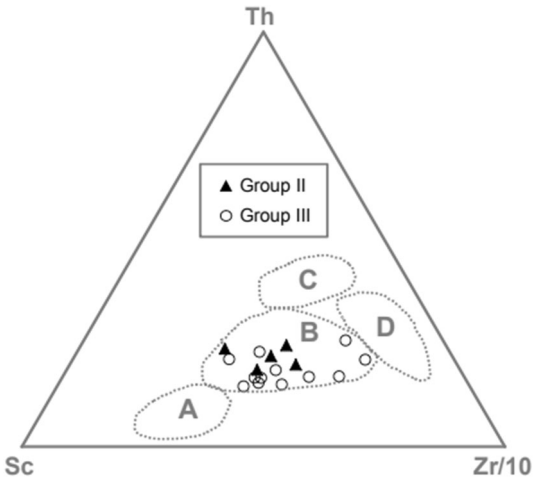

Fig. 7 Th–Sc–Zr/10 ternary diagram after Bhatia and Crook (1986) showing data from metapelites in the Kutjevo Zone. A—Oceanic island arc; B—Continental island arc; C—Active continental margin; D—Passive margin

Calculated single-point dates vary from 263 (±123) Ma to 631 (±129) Ma, but by far most dates are between 430 and 540 Ma with associated individual errors (2σ) typically of ± 70–90 Ma (Table 5). An exception is the mylonitic sample BS 423, where monazite ages below 400 Ma are frequently found (see below). Because the single-point dates generally overlap within error, it is interpreted that the analyses define one age population in each sample.

Calculated weighted mean ages for single samples also overlap within error and are between 465 ± 34 Ma (sample BS 203b) and 481 ± 26 Ma (sample BS 413a). The overall mean of all samples is 471 ± 15 Ma and is interpreted to constrain monazite growth in group III metapelites to the middle Ordovician. Notably, these monazite ages are significantly older than those published by Balen et al. (2006) for their locality from the same zone (444 ± 19 and 428 ± 25 Ma).

Xenotime is generally absent in group III metapelites (again with the exception of sample BS 423). The strongly varying and commonly moderately low Y contents in the monazite analyses indicate a general yttrium undersaturation. Applying Y-in-monazite thermometry, monazite grains with the highest measured Y contents (Y_2O_3 = 2 wt.%) yield crystallization temperatures of around 600 °C, similar to those obtained using other geothermobarometric methods for group III metapelitic rocks (see above).

The monazite grains in sample BS 423 (mylonitic shear band) mostly yield Variscan ages (weighted mean of 372 ± 26 Ma). In some monazite grains from this sample, remnant Ordovician cores were detected (Fig. 8d, Table 5). The Variscan monazite grains in sample BS 423 all have low Y_2O_3 contents (< 0.8 wt.%). Given the fact that xenotime is also present in the sample (Fig. 8d), these low Y contents in the Variscan monazite are consistent with growth at low-temperature conditions of around 400–450 °C. Interestingly, the monazite grains in sample BS 423 show apatite–epidote coronas indicating a late-stage, post-crystallization monazite consumption, similar to that described by Finger et al. (1998).

Group IV metapelitic rocks: Accessory monazite was found in two samples (BS 408a, BS 411c) and is of similar size and shape to that in group III metapelites. However, in group IV samples, many monazite grains are overgrown by an apatite–allanite corona. Most monazite crystals occur in the matrix, and some are enclosed in low-Ca garnet. There is a large variation in Th contents with values ranging from only ~ 1 wt.% (and extremely large age errors) up to about 17 wt.% ThO_2 (Table 5). The measured Th–U–Pb ages vary between 274 and 447 Ma, but by far most dates are between 300 and 400 Ma with individual errors of ~ 30–80 Ma (2σ). Almost identical weighted mean ages of 354 ± 16 Ma and 351 ± 14 Ma are calculated for the two investigated samples (Table 1). These age data are interpreted to record a single Variscan event, although it cannot be excluded that some older monazite relics remain unrecognized due to large analytical errors. The ages presented here overlap the monazite age obtained by Horváth et al. (2010) from the Gradište locality (356 ± 23 Ma). We interpret that the Variscan monazite crystallized (or recrystallized from a pre-existing monazite) close to the thermal peak of the Variscan PT evolution, and slow cooling in the andalusite stability field led to the formation of the secondary apatite/allanite coronas around the monazites (Finger et al. 1998).

Lu–Hf isotope analyses and garnet dating

Three garnet fractions and one whole-rock sample from the group II metapelitic rocks (sample BS 417) were analyzed for Lu–Hf isotopes (Table 4). The garnets are slightly zoned. However, the zonation is continuous and is interpreted to record one prograde growth phase between 7 kbar/830 ℃ and 9 kbar/850 ℃ (see Figs. 4a, 5a). All four analyses plot on an isochron (Fig. 9) with an age of 466.0 ± 2.3 Ma (MSWD = 1.8) and the latter is accepted as geologically meaningful (for more details, see discussion below). The whole-rock analysis yields $\varepsilon Hf_{466Ma} = -4.7 \pm 0.7$ (Table 4), indicating that the protolith of the metapelitic rock must have contained relatively old crustal components. This is reflected in a two-stage hafnium model age of 1.62 Ga.

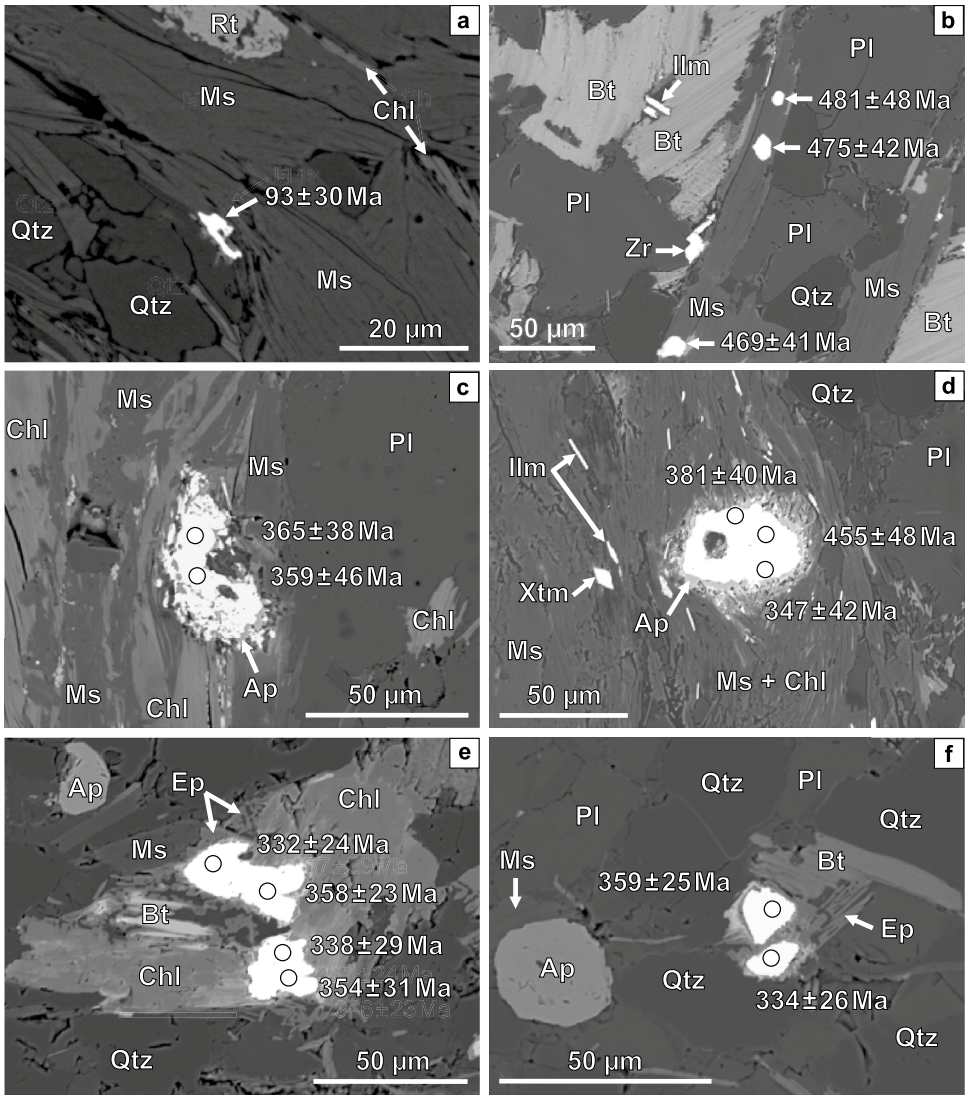

Fig. 8 BSE images of dated monazite grains (age errors 1σ): **a** Sample BS 606 (Group I); **b** Sample BS 420 (Group III); **c, d** Sample BS 423(Group III mylonite); **e, f** Sample BS 411c (Group IV)

Table 4 Results of Lu–Hf isotope dating of garnet (3 fractions) in sample BS 417 (wr = whole rock)

Fraction	Lu	Hf	$^{176}Lu/^{177}Hf$	±2 S.D	$^{176}Hf/^{177}Hf$	±2 S.D	Age	eHf_t	±2 sig	TDM
	(ppm)	(ppm)		(abs)		(abs)	(Ma)			
Grt0	5.6	1.0	0.8371	0.00209	0.289675	0.00002	466			
Grt1	3.7	1.2	0.4548	0.00114	0.286344	0.00003	466			
Grt1	3.3	1.2	0.4029	0.00101	0.285857	0.00002	466			
wr	0.3	1.1	0.0403	0.00010	0.282711	0.00002	466	− 4.7	0.7	1.62

Discussion

The polymetamorphic architecture of the Krndija region

Contrary to the frequently cited model of a monocyclic Variscan metamorphic evolution (Pamić and Lanphere 1991), it now becomes increasingly obvious that the Krndija area in the Slavonian Mountains records a complex, polymetamorphic history involving Sardic (Ordovician), Variscan, and Alpine metamorphic imprints. The EMP monazite age dates from this study not only highlight but place some regional constraints on this polymetamorphic evolution. We find the following monazite age distribution in the Krndija region (Figs. 2, 10):

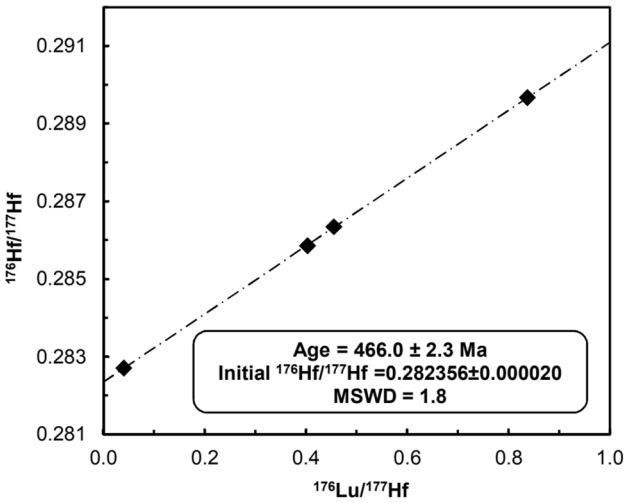

Fig. 9 Lu–Hf isochron diagram (whole-rock plus three garnet fractions) for sample BS 417 (group II metapelite)

1) Alpine monazite ages occur in the northern part of Krndija, in the so-called phyllite zone (i.e., group I metapelites).
2) Variscan monazite ages are recorded in group IV metapelites on the southern flank of the Krndija metamorphic complex that define a zone (herein termed the Gradište Zone) of penetrative, amphibolite facies grade, Variscan metamorphism.
3) Ordovician monazite ages are prominent in the intervening crustal strip (i.e., group III metapelites).

Notably, despite its only moderate precision, EMP-based monazite dating has proved to be a key method in revealing the complex geological history of the study area. Admittedly, it would appear at first sight that up to half of the measured single-point monazite ages are insignificant due to very high individual age uncertainties. However, even without any data screening, the overall statistics of the measured monazite dates fundamentally records a polymetamorphic evolution with Alpine, Variscan, and Ordovician age peaks (Fig. 10a). The geochronological constraints become tighter when very-high-error dates are omitted (Fig. 10b) and weighted average ages for single samples are considered (Fig. 10c, Table 5). However, as a precaution, the geological significance of such statistically optimized EMP monazite dates should always be confirmed by another geochronological method. In this study, a precise Lu–Hf garnet age of 466 ± 2.3 Ma was obtained for the (monazite–free) metapelites of group II, which reside between group III metapelites and the phyllite zone. This age is consistent with the average monazite age of 471 ± 15 Ma for the adjacent group III metapelites.

Based on all the geochronological information, we propose that a large geologically discrete composite zone, with

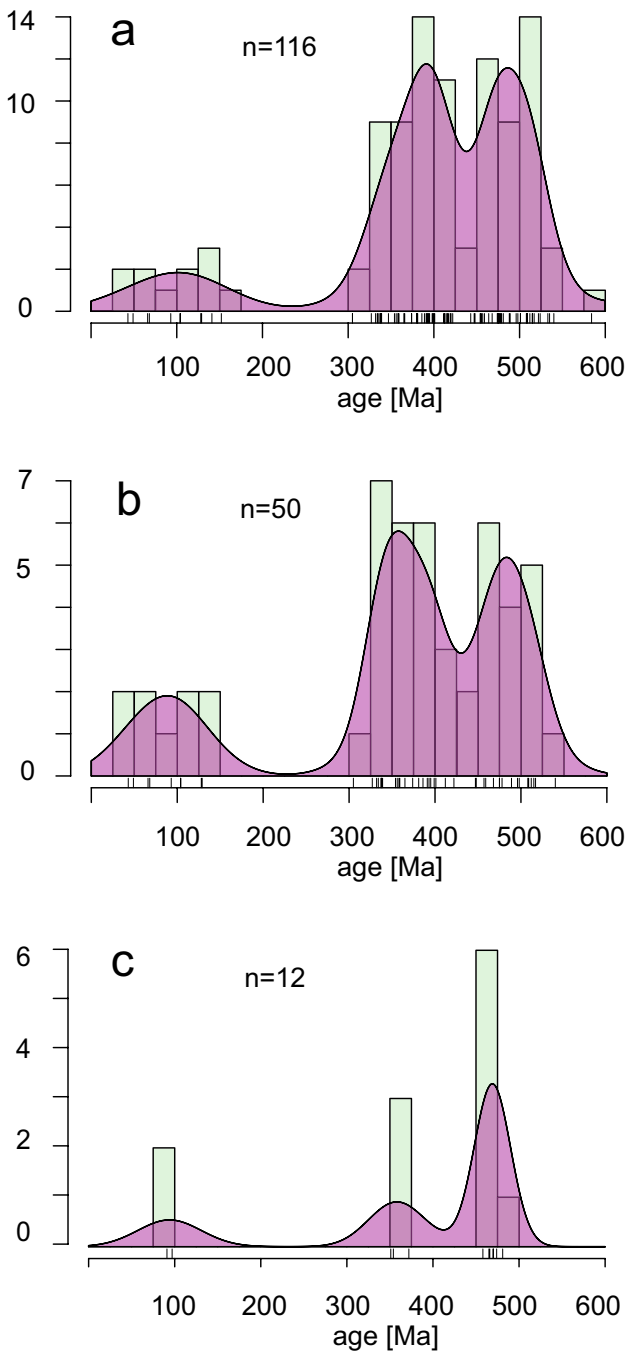

Fig. 10 Kernen density plots of the EMP monazite age data from all samples in this study: **a** all single-point ages; **b** single-point ages with errors < 50 Ma (1σ); **c** weighted average ages for the dated samples (see Table 5). See text for further explanation

well-preserved remnant Sardic metamorphic basement, is present in the central part of Krndija and has a minimum length of 23 km and is approximately 2 km wide (Fig. 2). Small amphibolite and metagranitoid lenses intercalated in group III metapelites (Balen et al. 2015) are most probably

Table 5 Th–U–Pb data for monazite (errors are 2σ)

	Th (wt%)	U (wt%)	Pb (wt%)	Age ± 2σ (Ma)		Th (wt%)	U (wt%)	Pb (wt%)	Age ± 2σ (Ma)
Group I metapelites					Group III metapelites				
Sample BS 502					Sample BS 203b				
m1	7.159	0.149	0.035	104 ± 59	m 1 dark	0.503	0.102	0.016	428 ± 535
m2	7.233	0.161	0.023	68 ± 58	m 1 bright	0.474	0.780	0.070	517 ± 147
m3	5.918	0.159	0.019	66 ± 70	m 2	3.485	1.022	0.146	478 ± 65
m4	5.933	0.184	0.038	129 ± 69	m 3a	3.398	0.851	0.124	448 ± 72
				91 ± 31	m 3b	4.059	0.871	0.141	457 ± 65
Sample BS 606					m 4	2.465	0.726	0.101	464 ± 92
m1	2.030	-0.023	0.012	141 ± 115					**465 ± 34**
m2	2.973	0.035	0.006	43 ± 73	Sample BS 423				
m3	2.811	-0.021	0.019	152 ± 82	m 1 P2	3.103	0.590	0.088	394 ± 89
m4	3.329	0.072	0.016	104 ± 63	m 1 P3	3.398	0.576	0.082	347 ± 85
m5	3.440	0.045	0.015	93 ± 60	m 1 P4	3.303	0.586	0.096	413 ± 86
m6	3.295	0.088	0.020	128 ± 63	m 1 P5	3.955	0.573	0.109	417 ± 77
m7	3.332	-0.001	0.007	49 ± 68	m 1 P6	3.869	0.530	0.095	381 ± 80
				97 ± 26	m 3	2.608	0.325	0.043	263 ± 123
Group III metapelites					m 5 P1	3.901	0.638	0.097	365 ± 75
Sample BS 413a					m 5 P2	3.031	0.572	0.078	359 ± 92
m 1 P1	0.487	1.114	0.084	454 ± 109	m 7 P1	3.319	0.516	0.089	400 ± 90
m 1 P2	0.556	1.090	0.099	535 ± 108	m 8 P2	4.205	0.533	0.081	305 ± 76
m 2	1.481	0.869	0.101	522 ± 103	m 8 P3	3.965	0.439	0.100	416 ± 83
m 3	2.888	0.753	0.114	477 ± 83					**372 ± 26**
m 4 P1	2.817	0.877	0.098	386 ± 79	Sample BS 423 (relictic grains)				
m 4 P2	2.787	0.796	0.116	479 ± 83	m 1 P7	2.926	0.526	0.095	455 ± 96
m 9 P1	3.716	0.790	0.134	475 ± 71	m 2	4.026	0.690	0.129	459 ± 71
m 9 P2	3.797	0.781	0.133	468 ± 70	m 6 core	2.933	0.570	0.102	476 ± 93
m 10	1.446	0.758	0.091	515 ± 113	m 7 P2	2.633	0.443	0.080	435 ± 110
m 11	1.543	0.803	0.100	533 ± 107					**458 ± 44**
m 12 P1	3.449	0.513	0.096	420 ± 87	Group IV metapelites				
m 12 P2	3.730	0.659	0.125	475 ± 76	Sample BS 408a				
				481 ± 26	m 1 P1	1.019	0.172	0.025	350 ± 284
Sample BS 201a					m 2	3.652	0.844	0.112	393 ± 70
m1	2.810	0.808	0.123	501 ± 82	m 3 P1	3.585	0.851	0.093	327 ± 71
m2	4.268	0.574	0.116	422 ± 73	m 3 P2	2.947	1.005	0.110	395 ± 72
m3	2.832	0.827	0.127	512 ± 80	m 3 P3	3.669	0.789	0.094	338 ± 72
				474 ± 45	m 4	3.253	0.549	0.094	415 ± 89
Sample BS 420					m 5	4.250	0.446	0.114	447 ± 78
m 1	1.559	0.357	0.045	374 ± 165	m 6	6.638	0.424	0.121	337 ± 56
m 2	2.616	0.278	0.077	488 ± 126	m 7	3.066	1.050	0.116	401 ± 69
m 3 bright	1.964	0.687	0.073	389 ± 107	m 8 rim	1.805	0.045	0.029	333 ± 229
m 3 dark	1.974	0.490	0.084	524 ± 125	m 8a	2.771	0.087	0.042	305 ± 147
m 5	1.950	0.513	0.090	548 ± 123	m 8a bright	16.808	0.549	0.282	339 ± 24
m 6	1.350	0.886	0.072	380 ± 106	m 8a dark	2.794	0.702	0.069	305 ± 89
m 7 bright	1.547	0.322	0.061	524 ± 171	m 9	4.000	0.956	0.113	356 ± 63
m 7 dark	0.846	0.454	0.057	543 ± 191					**354 ± 16**
m 10 bright	2.238	0.742	0.101	481 ± 96	Sample BS 411c				
m 10 dark	1.680	0.208	0.050	475 ± 189	m 1 P 1	2.412	0.506	0.064	354 ± 62
m 16	1.755	0.351	0.071	544 ± 153	m 1 P 2	4.869	0.895	0.127	338 ± 58
m 17	2.080	0.196	0.057	475 ± 84	m 2 P1	2.643	0.535	0.053	274 ± 103

Table 5 (continued)

	Th (wt%)	U (wt%)	Pb (wt%)	Age ± 2σ (Ma)		Th (wt%)	U (wt%)	Pb (wt%)	Age ± 2σ (Ma)
				470 ± 36	m 2 P2	6.023	0.476	0.135	399 ± 59
Sample BS 419b					m 3 dark	1.087	0.490	0.054	447 ± 184
m 1	3.336	0.197	0.068	380 ± 112	m 3 bright	1.051	0.437	0.043	393 ± 181
m 2 bright	5.944	0.184	0.144	489 ± 68	m 4	4.047	0.541	0.087	334 ± 52
m 2 dark	4.195	0.391	0.101	412 ± 82	m 5 P1	2.443	0.578	0.076	393 ± 108
m 3 core dark	4.966	0.289	0.103	391 ± 76	m 5 P2	1.373	0.273	0.038	376 ± 198
m 3 rim bright	4.054	0.242	0.096	443 ± 92	m 6	4.328	0.486	0.095	359 ± 50
m 4 core dark	2.872	0.354	0.067	374 ± 111	m 7	2.882	0.623	0.080	366 ± 91
m 5	4.145	0.130	0.097	474 ± 98	m 8 P1	17.254	0.518	0.281	332 ± 24
m 6	3.990	0.246	0.108	501 ± 93	m 8 P2	18.323	0.470	0.317	358 ± 23
m 7 core dark	3.120	0.380	0.101	515 ± 102	m 9	3.256	0.321	0.065	338 ± 105
m 7 rim dark	3.572	0.062	0.077	455 ± 118	m 23 core	1.958	0.403	0.053	363 ± 137
m 7 rim bright	4.772	0.280	0.127	496 ± 78	m 23 rim	1.493	0.269	0.042	397 ± 189
m 8	5.215	0.367	0.156	540 ± 69					**351 ± 14**
m 9	5.268	0.378	0.145	498 ± 69					
m 14 dark	4.816	0.173	0.123	508 ± 83					
m 14 bright	3.807	0.375	0.115	509 ± 89					
				471 ± 22					
Sample BS 203a									
m 1	2.990	0.938	0.141	517 ± 74					
m 2 core	3.943	0.364	0.142	611 ± 86					
m 2 rim	4.754	0.307	0.106	412 ± 78					
m 3	1.308	0.651	0.098	631 ± 129					
m 4 bright	2.996	0.563	0.085	392 ± 93					
m 4 dark	1.873	0.592	0.093	544 ± 117					
m 5 core	3.816	0.461	0.100	419 ± 84					
m 5 rim	3.942	0.399	0.093	398 ± 85					
m 6 core	2.436	0.889	0.124	515 ± 83					
m 6 rim	2.508	0.924	0.082	335 ± 82					
m 9	2.887	0.928	0.126	475 ± 75					
				466 ± 26					

Weighted average ages (bold) are at the 95% confidence level

also pieces of Sardic metamorphic basement. This composite Sardic complex in the Krndija zone, which we name the Kutjevo Zone, complements the Strona–Ceneri Zone (Zurbriggen et al. 1997), and should be recognized as a key region in any study of the "Sardic orogeny".

The Sardic record of the Kutjevo Zone

Our data support the pioneering conclusions of Balen et al. (2006) that the Slavonian Mountains host a pre-Variscan metamorphic component. However, the monazite ages published in Balen et al. (2006) were rather in favor of a late Ordovician or Silurian metamorphic event at about 440 Ma (although with very large error), whereas our data clearly support a middle Ordovician metamorphic event, which coincides with the so-called Sardic phase described in the other parts of the Alps (see Introduction section).

The peak T stage of the Sardic metamorphism in the Kutjevo Zone, which is represented by growth of garnet in group II and garnet rim zones in group III metapelites, took place at 540–620 °C and at relatively high-pressures of 9–12 kbar typical of a subduction zone setting. Based on the Lu–Hf garnet isochron age for sample BS 417, we propose that this Barrovian metamorphic event occurred around 466 Ma. Note that the dated garnets from this sample can be expected to provide a geologically meaningful Lu–Hf isochron age, because they are continuously zoned and likely formed one-phase prograde between 7 kbar/830 °C and 9 kbar/850 °C (see Fig. 4a, 5a).

A previous (slightly or perhaps even significantly older) metamorphic event (M1) with a different PT evolution is

recorded in garnet cores in the group III metapelites. The composition of these cores reveals a pre-HP stage of prograde isobaric heating at 7 kbar (Figs. 4b, 5b). The typically discontinuously zoned garnets experienced a growth break when passing through the 7–10 kbar pressure interval. Their rim zones record the Sardic high-pressure event in form of a clockwise *PT* evolution to peak *T* conditions of 580–620 °C and 9–10 kbar (Figs. 4b, 5b). Metastable staurolite, which is locally found in group III metapelites, is considered an M1 relict.

Horváth et al. (2010), who studied a sample of group III metapelites (also with low-Ca garnet cores), proposed a simple prograde PT evolution from 550 ℃ at 6 kbar to 640 ℃/12 kbar for this rock (thin dashed arrow in Fig. 5). However, such a PT trajectory is clearly not consistent with the observed M1 garnet core zoning (which shows no compression) and, is indeed inconsistent with the presence of early staurolite in the rock. Furthermore, a continuous zoning in Xgrs, Xsps, and Xpy would be expected in garnet growth during a simple prograde PT path but, instead, the garnet porphyroblasts in group III metapelites show an abrupt compositional change at the core–rim transition.

The age of the M1 metamorphism is so far unconstrained. It could be pre-Sardic (for instance of Cadomian age), in which case an exhumation stage between the M1 and the M2 event may be a realistic assumption (path 2 in Fig. 5b). On the other hand, the M1 event could also be explained in terms of a mid-crustal contact metamorphism caused by early Sardic magmatism (perhaps represented by amphibolite and orthogneiss lenses in the metapelites). In the latter case, an anticlockwise compressional PT evolution (path 1 in Fig. 5b) is very feasible. The observation that the M1 garnet cores are widely unresorbed (euhedral) may lend some support to the latter model, but any further discussion on this matter must await robust and precise geochronological data on the formation ages of the surrounding amphibolites and orthogneisses, which are as yet not available.

The accurate time difference between M1 and M2 could perhaps be resolved in the future by attempting to directly date the M1 staurolite using U–Pb methods or by attempting to carefully separate the Ca-poor garnet cores for Lu–Hf dating. Also, the monazite in group III metapelites could record both events. Considering the work of Spear (2010), we assume that metasedimentary rocks like group III metapelites, with low-to-moderate CaO contents < 1.8 wt. % (Fig. 6), have a wide monazite stability field, which spans the PT conditions of both M1 and M2. Thus, a first monazite growth event could theoretically have occurred during M1 and a second growth or recrystallization event during M2. However, based on the observation that only a few monazite grains are enclosed in the garnet (and only in garnet rim zones), we conclude that the main phase of monazite growth in group III metapelites took place close to the T climax of the M2 event, i.e., after the M2 peak-P stage. The calculated weighted average ages (Fig. 10c) should, therefore, be tentatively interpreted as such, i.e., until further data are available, for example from more precise (e.g., SIMS-based) in-situ dating of monazite.

Another question that requires clarification in a future study concerns the apparent lithological division of the Kutjevo Zone into chlorite-rich (biotite-free) group II metapelites and biotite-bearing group III metapelites. This is unlikely to be just the result of variations in metamorphic grade, as stated by Pamić and Lanphere (1991). Our study shows that there is no pronounced hiatus in the metamorphic grade: the peak metamorphic conditions recorded in the biotite-free, chlorite-bearing group II metapelites are only slightly below those recorded in the biotite-bearing group III metapelites (540–570 °C/8–9 kbar vs. 570–620 °C/8–12 kbar). It is proposed here that the given petrographic contrasts (chlorite vs biotite assemblages) result mainly from bulk rock chemical differences (Fig. 6, Table 3), i.e., higher Al-contents and lower X_{Fe} in group II metapelites have stabilized chlorite instead of biotite. Obviously, we are dealing with two different sedimentary formations on the active Gondwana margin, as such, determination of the deposition ages via detrital zircon dating would be worthwhile.

The Variscan event

Traces of the Variscan orogeny are mainly recorded in the Gradište Zone. Our petrological data suggest that this zone underwent a clockwise *PT* evolution at medium-to-lower grade amphibolite facies conditions during the early Carboniferous (at ca. 355 Ma). The Variscan *PT* loop is characterized by a prograde *PT* increase from 530 ℃/ 5 kbar to 570 ℃/ 6 kbar (metamorphic peak), followed by a *PT* decrease to 550 ℃ at 3 kbar (Table 1).

Rare Ca-rich cores in some garnet porphyroblasts of group IV metapelitic rocks (Figs. 4c, 5c) represent probable relics of a pre-Variscan higher-P metamorphism. Considering the PT conditions, we assume that these garnet cores are Sardic in age. It is thus proposed that the Gradište Zone originally belonged, at least in part, to the Sardic metamorphic complex.

An interesting question arises as to how the Variscan orogeny affected the Kutjevo Zone. As stated earlier, monazite grains in lower-to-middle greenschist facies mylonitic rocks of the Kutjevo Zone record Variscan ages (sample BS423). This implies that at least parts of the Kutjevo Zone experienced low-grade metamorphic conditions during the Variscan orogeny (Table 1). However, the Variscan reheating obviously did not result in an appreciable recrystallization of the Kutjevo Zone rocks, as can be inferred from the low degree of retrogression of the Sardic high-P assemblage and the preservation of Ordovician monazite ages.

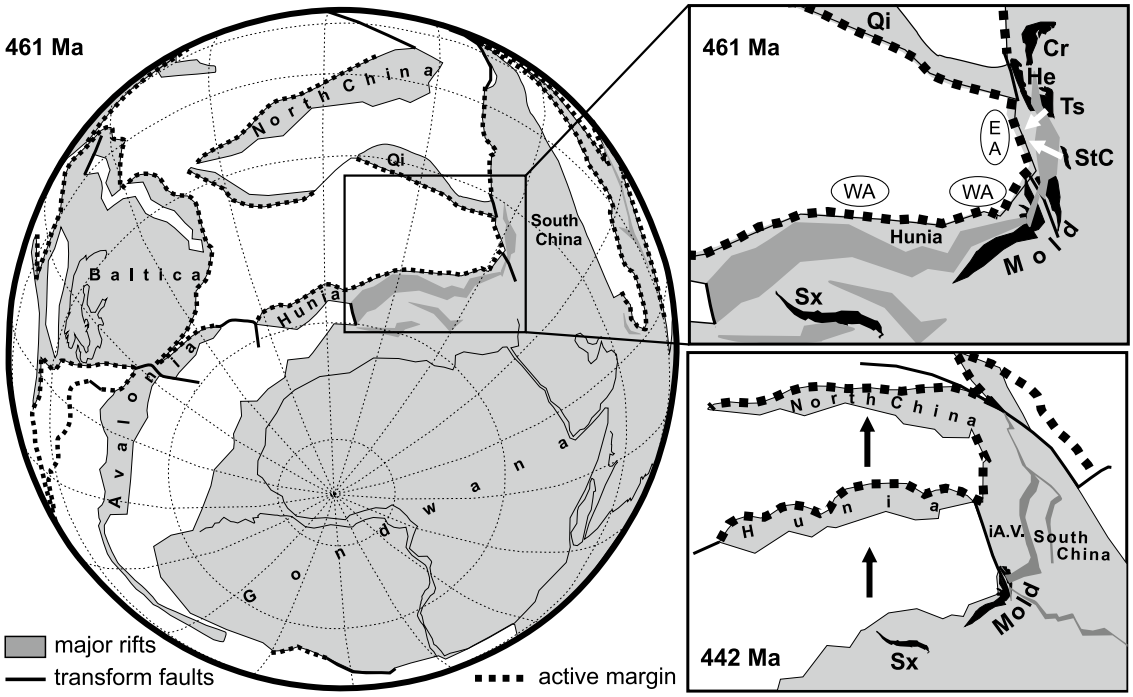

Fig. 11 Palaeogeography of the Late Ordovician after Stampfli et al. (2013). *EA* East-Armorican (now intra-Alpine) segment of the Gondwana margin with strong imprints of the Sardic orogeny (subduction), *WA* West Armorican segment of the Gondwana margin with missing or weak imprints of the Sardic orogeny (transpressional–transtensional). See further explanations in text. *Cr* Carpathians, *He* Helvetic (with Gotthart Massif), *Mold* Massif Central/Moldanubian zone, *StC* Strona-Ceneri, *Sx* Saxothuringia, *Ts*Tisia, *iA.V* intra-Alpine Variscan basement

Another interesting question is whether the phyllite zone experienced Variscan metamorphism. High-grade metamorphic mineral relics are not observed in these rocks, so any metamorphic overprint must have been low grade. If the protoliths of the phyllites were indeed Upper Devonian sedimentary rocks, as proposed by Jamičić (1983) and Jamičić and Brkić (1987), then a continuous Variscan metamorphic zonation could exist in Krndija from amphibolite facies grade in the south (Gradište Zone) over low grade (greenschist facies) in the Kutjevo Zone to very low grade in the northern Phyllite Zone. On the other hand, it is also possible that the protoliths of the phyllites were deposited in post-Variscan times; for example, during the Upper Carboniferous, Permian or Mesozoic. Dating of detrital zircons would be necessary to solve this question.

The Alpine event

Results of monazite dating and petrographic observations indicate that the phyllites in northern Krndija crystallized in the Cretaceous under low-to-middle greenschist facies conditions (Table 1).

We speculate that the older, higher grade basement units of Krndija (the Kutjevo and Gradište Zones) also experienced a low-grade heating event during the Cretaceous, although this is difficult to confirm using the current geochronometric methods. Local chlorite-bearing shear zones with an S2 foliation in the basement rocks (Balen et al. 2006) could well have formed during the Alpine event (but alternatively also during the Variscan). Nevertheless, the generally unaltered nature of the Sardic mineral parageneses in the Kutjevo zone (group II and III metapelites) allows for the conclusion that Alpine metamorphism only barely affected the crystalline basement of Krndija.

Comparison of the Kutjevo Zone with the Strona-Ceneri Zone and palaeogeographic implications

It is undeniable that there are striking petrographical parallels between the Strona-Ceneri Zone and the Kutjevo Zone. First, there is the lithological association, which is in both cases clearly dominated by metapelitic (metagreywacke) rocks with a pre-middle Ordovician formation age. These metasediments are inter-layered with numerous small

amphibolitic units as well as metagranitoids. According to Zurbriggen et al. (2017), the latter may represent syntectonic I-type granitoids of Ordovician age.

In addition, both areas received their main deformation during an Ordovician Barrow-type metamorphic event and lack signs of significant post-orogenic (Ordovician) reequilibration at $P < 7$ kbar. Ordovician eclogite facies metamorphism as recorded in the Strona-Ceneri Zone (Franz and Romer 2007) is so far not found in Krndija. However, it should be mentioned that the amphibolitic rocks of Krndija, which are considered the most likely to contain eclogite relics, are still not well investigated. Garnet core compositions in the Kutjevo Zone metapelites may be interpreted in terms of syn-compressional contact metamorphism and syntectonic magmatism, respectively (see above). This would match the tectonothermal situation that Zurbriggen (2017) has proposed for the Strona-Ceneri Zone.

Zurbriggen et al. (1997, 2017) interpreted the Strona-Ceneri Zone as a Cambro-Ordovician fore-arc complex that was subducted in the middle Ordovician. A similar scenario is also feasible for the Kutjevo Zone, because (i) the metapelitic rocks in the Kutjevo Zone are also associated with amphibolites with MORB signatures, and (ii) they were, according to geochemical data, most likely deposited along an active continental margin (Fig. 7).

There is wide agreement today that the pre-Variscan intra-Alpine basement units are mainly derived from an eastern segment of the northern Gondwana margin. They may have resided either adjacent to South China (von Raumer et al. 2013) or in front of the Arabian–Nubian Shield and the Sahara craton (Siegesmund et al. 2021; Finger and Riegler 2022). Also, there is wide agreement that large parts of the northern Gondwana margin had an Andean-type character during the Cadomian orogeny (e.g., Nance et al. 2008; von Raumer et al. 2013). However, it remains controversial whether and to what extent this Cadomian Andean-type setting persisted into the Ordovician. Many geologists believe that subduction had widely ceased by the late Cambrian and that most of the northern Gondwana margin became a passive margin in the Ordovician (see, e.g., Žák and Sláma 2018 and further references therein). Indeed, evidence for Ordovician subduction-related metamorphism is fairly rare in central Europe. Until now, such evidence was reported only from a few intra-Alpine regions with the Strona-Ceneri Zone as the most prominent example (Faryad et al. 2002; Biino 1995; Zurbriggen et al. 1997; Handy et al. 1999).

We can now present further data in favor of a Sardic subduction scenario from the Slavonian Mountains in Croatia. This region is almost 1000 km away from the Strona-Ceneri Zone. However, considering the palaeogeographic reconstructions of Stampfli et al. (2013), both units were situated relatively closely together in Ordovician times (Fig. 11). In the palaeogeographic map for the middle Ordovician (461 Ma) by Stampfli et al. (2013), the positions of both units are located somewhat remote from the Gondwana plate edge, to the east behind a large Ordovician back-arc rift and adjacent to South China (Fig. 11). However, prior to the back-arc rifting, they could have been positioned much closer to the Gondwana plate margin (note arrows in Fig. 11) and an Alaskan-type subduction–accretion scenario as proposed by Zurbriggen (2015) is absolutely feasible.

It is important to note that Stampfli et al. (2013) support the notion that an extended Ordovician Cordillera did exist along the northern Gondwana margin (Fig. 11). They suggest that much of this Cordillera was later detached from Gondwana along with the Hunic ribbon terrane, and finally became part of Asia (Fig. 11). Based on this model, the intra-Alpine basement terranes with Sardic metamorphism could be interpreted as Cordillera relics that remained connected to Gondwana throughout the Early Palaeozoic and later became part of the Variscan collision zone.

However, the Hunia terrane model as such can be fundamentally challenged, since several distal (i.e., ocean near) segments of the Cadomian orogen are distributed over both the Alps (Siegesmund et al. 2021; Neubauer et al. 2022) and the Bohemian Massif (Žák and Sláma 2018), a fact which would argue against a Cordillera loss. Apart from that, the concept of a persistent Cadomian–Ordovician subduction zone along the entire north Gondwana margin (Stampfli et al. 2013) is disclaimed by numerous geologists, who argue instead in favor of a predominantly passive margin setting in the Ordovician (e.g., Franke et al. 2017). Indeed, regions with Sardic orogenic imprints outside of the Alps (e.g., Alvaro et al. 2016; Casas 2010; Cocco and Funedda 2017) do not show evidence for subduction and could be explained in terms of transpressional–transtensional tectonics along the north Gondwana margin as well.

A viable compromise that we suggest here is to invoke an (Alaskan-type?) Ordovician subduction setting only for a distinct eastern segment of the north Gondwana margin, which we may term E-Armorica following Finger and Riegler (2022) and which is now mainly exposed in the Alps (Fig. 11). In this scenario, the more western parts of frontal north Gondwana (W-Armorica according to Finger and Riegler 2022, see Fig. 11) had already undergone a change from an active to a transtensional–transpressional passive margin setting by the end of the Cambrian.

Conclusions

1) The Krndija region of the Slavonian Mountains, Croatia, was affected by at least three major tectonometamorphic imprints: during the Middle Ordovician (Sardic event), the Early Carboniferous (Variscan event), and the Cretaceous (Alpine event).

2) Based on monazite dating and thermobarometric studies on metapelitic rocks, three tectonometamorphic zones can be delineated in Krndija: the Kutjevo Zone with well-preserved medium-grade Ordovician basement, the Gradište Zone with penetrative medium-grade Variscan metamorphism, and the Phyllite Zone with low-grade Alpine metamorphism.
3) The Sardic metamorphic event in the Kutjevo Zone is additionally confirmed by a precise Lu–Hf garnet-whole-rock isochron age of 466.0 ± 2.3 Ma.
4) The Kutjevo Zone is recognized as a key region for the study of the Sardic (Ordovician) orogeny. It shows striking similarities to the Strona-Ceneri Zone in the western Alps in terms of lithology and metamorphic history.
5) We suggest a tectonic scenario where the E-Armorican (now intra-Alpine) sector of the northern Gondwana margin experienced a subduction setting in the middle Ordovician, while the W-Armorican segment (now exposed in the French, German and Czech Variscides) had already mutated from a (Cadomian) subduction setting to an extensional (transtensional–transpressional) setting by the late Cambrian.

Acknowledgements We thank Gernold Zulauf, a second anonymous reviewer, and editors Ulrich Riller and Albrecht von Quadt for the helpful comments, and Noreen Vielreicher for linguistic improvements on the text. Parts of the work received support through FWF project P18070 (to F.F.).

Funding Open access funding provided by Paris Lodron University of Salzburg.

Data availability The datasets generated and analyzed during the current study are available from the corresponding author on reasonable request.

References

Alvaro JJ, Colmenar J, Monceret E, Pouclet A, Vizcalino D (2016) Late Ordovician (post-Sardic) rifting branches in the North Gondwanan Montagne Noire and Mouthoumet massifs of southern France. Tectonophysics 681:111–123

Balen D, Horváth P, Tomljenovic B, Finger F, Humer B, Pamic J, Arkai P (2006) A record of pre-Variscan Barrovian regional metamorphism in the eastern part of the Slavonian Mountains (NE Croatia). Mineral Petrol 87:143–162

Balen D, Horváth P, Finger F, Starijaš Mayer B (2013) Phase equilibrium, geothermobarometric and xenotime age dating constraints on the Alpine metamorphism recorded in chloritoid schists from the southern part of the Tisia Mega-Unit (Slavonian Mts., NE Croatia). Int J Earth Sci 102:1091–1109

Balen D, Massonne HJ, Petrinec Z (2015) Collision-related Early Paleozoic evolution of a crustal fragment from the northern Gondwana margin (Slavonian Mountains, Tisia Mega-Unit, Croatia): Reconstruction of the P-T path, timing and paleotectonic implications. Lithos 232:211–228

Bhatia MR, Crook KA (1986) Trace element characteristics of graywackes and tectonic setting discrimination of sedimentary basins. Contrib Miner Petrol 92(2):181–193

Bhattacharya A, Mohanty L, Maji A, Sen SK, Raith M (1992) Non-ideal mixing in the phlogopite-annite binary: constraints from experimental data on Mg− Fe partitioning and a reformulation of the biotite-garnet geothermometer. Contrib Miner Petrol 111(1):87–93

Biino GG (1995) Pre-Variscan evolution of the eclogitised mafic rocks from the Helvetic basement of the central Alps. Eur J Mineral 1995:57–70

Biševac V, Balen D, Tibljaš D, Španić D (2009) Preliminary results on degree of thermal alteration recorded in the eastern part of Mt. Papuk, Slavonia Croatia. Geologia Croatica 62(1):63–72

Biševac V, Krenn E, Balen D, Finger F, Balogh K (2011) Petrographic, geochemical and geochronological investigation on granitic pebbles from Permotriassic metasediments of the Tisia terrain (eastern Papuk, Croatia). Mineral Petrol 102:162–108

Biševac V, Krenn E, Finger F, Luzar-Oberiter B, Balen D (2013) Provenance of Paleozoic very low- to low-grade metasedimentary rocks of South Tisia (Slavonian Mountains, Radlovac Complex, Croatia). Geol Carpath 64(1):3–22

Blichert-Toft J, Chauvel C, Albarède F (1997) Separation of Hf and Lu for high-precision isotope analysis of rock samples by magnetic sector-multiple collector ICP-MS. Contrib Mineral Petrol 127:248–260

Bouvier A, Vervoort JD, Patchett PJ (2008) The Lu–Hf and Sm–Nd isotopic composition of CHUR: constraints from unequilibrated chondrites and implications for the bulk composition of terrestrial planets. Earth Planet Sci Lett 273:48–57

Bussy F, von Raumer J (1994) U-Pb geochronology of Palaeozoic magmatic events in the Mont-Blanc CrystallineMassif, Western Alps. Schweiz Mineral Petrogr Mitt 74:514–551

Casas JM (2010) Ordovician deformations in the Pyrenees: new insights into the significance of pre-Variscan ('sardic') tectonics. Geol Mag 147:674–689

Cocco F, Funedda A (2017) The Sardic Phase: field evidence of Ordovician tectonics in SE Sardinia, Italy. Geol Mag 156:25–38

Coggon R, Holland TJB (2002) Mixing properties of phengitic micas and revised garnet-phengite thermobarometers. J Metamorph Geol 20(7):683–696

Csontos L (1995) Tertiary tectonic evolution of the Intra-Carpathian area: a review. Acta Vulcanol 7(2):1–13

Csontos L, Vörös A (2004) Mesozoic plate tectonic reconstruction of the Carpathian region. Palaeogeog Palaeoclim Palaeoecol 210:1–56

Eichhorn R, Loth G, Kennedy A (2001) Unravelling the pre-Variscan evolution of the Habach terrane (Tauern Window. Austria) by U-Pb SHRIMP zircon data. Contrib Miner Petrol 142:147–162

Faryad SW, Melcher F, Hoinkes G, Puhl J, Meisel T, Frank W (2002) Relics of eclogite facies metamorphism in the Austroalpine

basement, Hochgrössen (Speik complex). Austria Mineral Petrol 74(1):49–73
Finger F, Riegler G (2022) Is there an Upper Devonian rift zone under the northern front of the Alps separating East and West Armorican crustal segments? Geol Carpathica 73(3):81–185
Finger F, Broska I, Roberts MP, Schermaier A (1998) Replacement of primary monazite by apatite-allanite-epidote coronas in an amphibolite facies granite gneiss from the eastern Alps. Am Miner 83(3–4):248–258
Fodor L, Csontos L, Bada G, Györfi I, Benkovics L (1999) Tertiary tectonic evolution of the Pannonian Basin system and neighbouring orogens: a new synthesis of palaeostress data. In: Durand D, Jolivet L, Horváth F, Séranne M (eds) The mediterranean basins: tertiary extension within the Alpine Orogen, vol 156. Geological Society Special Publications, London, pp 295–334
Franke W, Haak V, Oncken O, Tanner D (eds) (2000) Orogenic processes: quantification and modelling in the Variscan Belt. Geological Society, London, Special Publications, p 179
Franke W, Cocks LRM, Torsvik TH (2017) The Palaeozoic Variscan oceans revisited. Gondwana Res 48:257–284
Franz L, Romer RL (2007) Caledonian high-pressure metamorphism in the Strona-Ceneri Zone (Southern Alps of southern Switzerland and Northern Italy). Swiss J Geosci 100:457–467
Gaidies F, De Capitani C, Abart R (2008) THERIA_G: a software program to numerically model prograde garnet growth. Contrib Miner Petrol 155(5):657–671
Géczy B (1973) The origin of the Jurassic faunal provinces and the Mediterranean plate tectonics. Ann. Univ Sci Budapest r, Eötvös Nom Sect Geol 16:99–114
Gerdes A, Zeh A (2006) Combined U-Pb and Hf isotope LA-(MC)-ICP-MS analyses of detrital zircons: comparison with SHRIMP and new constraints for the provenance and age of an Armorican metasediment in Central Germany. Earth Planet Sci Lett 249:47–61
Haas J, Péró C (2004) Mesozoic evolution of the Tisza Mega-unit. Int J Earth Sci 93:297–313
Handy MR, Franz L, Heller F, Janott B, Zurbriggen R (1999) Multistage accretion and exhumation of the continental crust (Ivrea crustal section, Italy and Switzerland). Tectonophysics 18:1154–1177
Heinrich W, Rehs G, Franz G (1997) Monazite–xenotime miscibility gap thermometry I An empirical calibration. J Metamorph Geol 15(1):3–16
Holland TJB, Powell R (1990) An enlarged and updated internally consistent thermodynamic dataset with uncertainties and correlations: the system K2O–Na2O–CaO–MgO–MnO–FeO–Fe2O3–Al2O3–TiO2–SiO2–C–H2–O2. J Metamorph Geol 8(1):89–124
Holland TJB, Powell R (1998) An internally consistent thermodynamic data set for phases of petrological interest. J Metamorph Geol 16(3):309–343
Holland T, Powell R (2003) Activity–composition relations for phases in petrological calculations: an asymmetric multicomponent formulation. Contrib Miner Petrol 145(4):492–501
Horváth P, Balen D, Finger F, Tomljenović B, Krenn E (2010) Contrasting P-T–t paths from the basement of the Tisia Unit (Slavonian Mts., NE Croatia): application of quantitative phase diagrams and monazite age dating. Lithos 117:269–282
Jamičić D (1983) Strukturni sklop metamorfnih stijena Krndije i južnih padina Papuka (Structural fabric of the metamorphosed rocks of Mt. Krndija and the eastern part of Mt. Papuk). Geol Vjesnik Zagreb 36:51–72 (**In Croatian**)
Jamičić D (1988) Strukturni sklop slavonskih planina (Tectonics of the Slavonian Mts.). PhD Thesis, University of Zagreb, 152 p (**In Croatian**)
Jamičić D (1989) Basic geological map of Yugoslavia in scale 1:100.000, sheet Daruvar. Geol Inst Zagreb, Fed Geol Inst Beograd
Jamičić D, Brkić M (1987) Basic geological map of Yugoslavia in scale 1:100.000, sheet Orahovica. Geol Inst Zagreb, Fed Geol Inst et Beograd
Jamičić D, Brkić M, Crnko J, Vragović M (1986) Basic geological map of Yugoslavia—Explanatory notes for sheet Orahovica. Geol Inst Zagreb, Fed Geol Inst Beograd, p 72
Jercinovic MJ, Williams ML (2005) Analytical perils (and progress) in electron microprobe trace element analysis applied to geochronology: background acquisition, interferences, and beam irradiation effects. Am Miner 90:526–546
Krenn E, Finger F (2004) Metamorphic formation of Sr-apatite and Sr-bearing monazite in a high-pressure rock from the Bohemian Massif. Am Miner 89(8–9):1323–1329
Krenn E, Ustaszewski K, Finger F (2008) Detrital and newly formed metamorphic monazite in amphibolite-facies metapelites from the Motajica Massif, Bosnia. Chem Geol 254:164–174
Lagos M, Scherer EE, Tomaschek F, Münker C, Keiter M, Berndt J, Ballhaus C (2007) High precision Lu–Hf geochronology of Eocene eclogite-facies rocks from Syros, Cyclades, Greece. Chem Geol 243:16–35
Linnemann U, McNaughton NJ, Romer RL, Gehmlich M, Drost K, Tonk C (2004) West African provenance for Saxo-Thuringia (Bohemian Massif): did Armorica ever leave pre-Pangean Gondwana? U/Pb-SHRIMP zircon evidence and the Nd-isotope record. Int J Earth Sci 93:683–705
Ludwig K (2007) Isoplot/Ex version 3.41b, a geochronological toolkit for Microsoft Excel. Berkeley Geochronology Center Special Publication No. 4.
Montel JM, Foret S, Veschambre M, Nicollet C, Provost A (1996) Electron microprobe dating of monazite. Chem Geol 131:37–53
Münker C, Weyer S, Scherer EE, Mezger K (2001) Separation of high field strength elements (Nb, Ta, Zr, Hf) and Lu from rock samples for MC-ICPMS measurements. Geochem Geophys Geosyst. https://doi.org/10.1029/2001GC000183
Nance RD, Murphy JB, Strachan RA, Keppie JD, Gutiérrez-Alonso G, Fernández-Suárez J, Quesada C, Linnemann U, D'Lemos R, Pisarevsky SA (2008) Neoproterozoic–early Palaeozoic tectonostratigraphy and palaeogeography of the peri-Gondwanan terranes: Amazonian v. West African connections. Geol Soc Lond Spec Publ 297:345–383
Neubauer F, Liu Y, Dong Y, Chang R, Genser J, Yuan S (2022) Pre-Alpine tectonic evolution of the Eastern Alps: from prototethys to paleotethys. Earth Sci Rev 226:103923
Pamić J, Jamičić D (1986) Metabasic intrusive rocks from the Paleozoic Radlovac complex of Mt. Papuk in Slavonija (northern Croatia). Rad Jugosl Akad Znan Umjet 424(21):97–125
Pamić J, Jurković I (2002) Paleozoic tectonostratigraphic units in the northwest and central Dinarides and the adjoining South Tisia. Intern J Earth Sci 91:538–554
Pamić J, Lanphere M (1991) Hercynian granites and metamorphic rocks from the Papuk, Psunj, Krndija and the surrounding basement of the Pannonian Basin (Northern Croatia, Yugoslavia). Geol Ljubl 34:81–253
Pamić J, Lanphere M, McKee E (1988) Radiometric ages of metamorphic and associated igneous rocks of the Slavonian Mountains in the southern part of the Pannonian Basin, Yugoslavia. Acta Geol Zagreb 18:13–39
Pamić J, Lanphere M, Belak M (1996) Hercynian I-type and and S-type granitoids from the Slavonian Mountains (southern Pannonian, north Croatia). N Jb Miner Abh 171:155–186
Pamić J, Balen D, Tibljaš D (2002) Petrology and geochemistry of orthoamphibolites from the Variscan metamorphic sequences of

the South Tisia in Croatia—an overview with geodynamic implications. Int J Earth Sci 91:787–798
Pin Ch, Marini F (1993) Early Ordovician continental break-up in Variscan Europe: Nd-Sr isotope and trace element evidence from bimodal igneous associations of the Southern Massif Central, France. Lithos 29:177–196
Poller U, Nägler TF, Liebetrau V, Galetti G (1997) Geochemical and Sm-Nd Characteristics of a polymetamorphic S-type granitoid: The Mönchalpgneiss-Silvretta nappe/Switzerland. Eur J Mineral 9(2):411–422
Pyle JM, Spear FS, Wark DA (2002) Electron microprobe analysis of REE in apatite, monazite and xenotime: protocols and pitfalls. Rev Mineral Geochem 48(1):337–362
Schaltegger U, Gebauer D (1999) Pre-Alpine geochronology of the Central, Western and Southern Alps. Schweiz Mineral Petrogr Mitt 79:79–87
Scherer E, Münker C, Mezger K (2001) Calibration of the lutetium-hafnium clock. Science 293:683–687
Schmid D, Bernoulli B, Fügenschuh L, Matenco S, Schefer R, Schuster M, Tischler K, Ustaszewski K (2008) The Alps-Carpathians-Dinarides connection: a correlation of tectonic units. Swiss J Geosci 101:139–183
Schulz B (2021) Petrochronology of monazite-bearing garnet micaschists as a tool to decipher the metamorphic evolution of the Alpine basement. Minerals 11(9):981
Schulz B, Bombach K, Pawlig S, Brätz H (2004) Neoproterozoic to early-Palaeozoic magmatic evolution in the Gondwana-derived Austroalpine basement to the south of the Tauern Window (Eastern Alps). Int J Earth Sci 93:824–843
Siegesmund S, Oriolo S, Schulz B, Heinrichs T, Basei MAS, Lammerer B (2021) The birth of the Alps: Ediacaran to Paleozoic accretionary processes and crustal growth along the northern Gondwana margin. Int J Earth Sci 110(4):1321–1348
Söderlund U, Patchett JP, Vervoort JD, Isachsen CE (2004) The 176Lu decay constant determined by Lu-Hf and U-Pb isotope systematics of Precambrian mafic intrusions. Earth Planet Sci Lett 219:311–324
Spear FS (2010) Monazite–allanite phase relations in metapelites. Chem Geol 279:55–611
Stampfli GM, Hochard C, Vérard C, Wilhem C (2013) The formation of Pangea. Tectonophysics 593:1–19
Starijaš Mayer B, Krenn E, Finger F (2013) Microcrystals of Th-rich monazite (La) with a negative Ce anomaly in metadiorite and their role for documenting Cretaceous metamorphism in the Slavonian Mountains (Croatia). Mineral Petrol 108:231–243
Stille H (1939) Bemerkungen betreffend die "Sardische" Faltung und den Ausdruck "Ophiolithisch." Zeitschrift Der Deutschen Geologischen Gesellschaft 91:771–773
Teichmüller R (1931) Zur Geologie des Thyrrhenisgebietes, Teil 1: Alte und junge Krustenbewegungen im südlichen Sardinien. Abhandlungen der wissenschaftlichen Gesesellschaft Göttingen. Math Phys Kl. 3:857–950
Thöni M (1999) A review of geochronological data from the Eastern Alps. Schweiz Mineral Petrogr Mitt 79(1):209–230
Vermeesch P (2018) IsoplotR: a free and open toolbox for geochronology. Geosci Front 9(5):1479–1493
Vervoort JD, Patchett PJ, Söderlund U, Baker M (2004) Isotopic composition of Yb and the determination of Lu concentrations and Lu/Hf ratios by isotope dilution using MC ICPMS. Geochem Geophys Geosyst. https://doi.org/10.1029/2004GC000721
von Quadt Q (1992) U-Pb zircon and Sm—Nd geochronology of mafic and ultramafic rocks from the central part of the Tauern Window (eastern Alps). Contr. Mineral. and Petrol. 110:57–67
von Raumer JF, Bussy F, Schaltegger U, Schulz B, Stampfli GM (2013) Pre-Mesozoic Alpine basements—their place in the European Paleozoic framework. Geol Soc Am Bull 125:89–108
Wimmenauer W (1984) Das prävariskische Kristallin im Schwarzwald. Fortschritte Der Mineralogie Beiheft 62(2):69–86
Žák J, Sláma J (2018) How far did the Cadomian 'terranes' travel from Gondwana during early Palaeozoic? A critical reappraisal based on detrital zircon geochronology. Int Geol Rev 60(3):319–338
Zeh A, Gerdes A (2014) HFSE-transport and U-Pb-Hf isotope homogenization mediated by Ca-bearing aqueous fluids at 2.04 Ga: constraints from zircon, monazite, and garnet of the Venetia Klippe, Limpopo Belt South Africa. Geochim Cosmochim Acta 138:81–100
Zurbriggen R (2017) The Cenerian orogeny (early Paleozoic) from the perspective of the Alpine region. Int J Earth Sci 106:517–529
Zurbriggen R, Franz L, Handy M (1997) Pre-Variscan deformation, metamorphism and magmatism in the Strona-Ceneri Zone (southern Alps of northern Italy and southern Switzerland). Schweiz Mineral Petrogr Mitt 77:361–380